

1 **A dataset of energy, water vapor and carbon exchange observations**
2 **in oasis-desert areas from 2012 to 2021 in a typical endorheic basin**

3
4 Shaomin Liu¹, Ziwei Xu¹, Tao Che², Xin Li³, Tongren Xu¹, Zhiguo Ren²,
5 Yang Zhang², Junlei Tan², Lisheng Song⁴, Ji Zhou⁵, Zhongli Zhu¹, Xiaofan
6 Yang¹, Rui Liu⁶, Yanfei Ma⁷

7 *Correspondence to:* Shaomin Liu (smliu@bnu.edu.cn), Ziwei Xu (xuzw@bnu.edu.cn)

8
9 ¹State Key Laboratory of Earth Surface Processes and Resource Ecology, Faculty of Geographical
10 Science, Beijing Normal University, Beijing 100875, China

11 ²Northwest Institute of Eco-Environment and Resources, Chinese Academy of Sciences, Lanzhou
12 730000, China

13 ³National Tibetan Plateau Data Center, State Key Laboratory of Tibetan Plateau Earth System and
14 Resources Environment, Institute of Tibetan Plateau Research, Chinese Academy of Sciences,
15 Beijing 100101, China

16 ⁴Key Laboratory of Earth Surface Processes and Regional Response in the Yangtze-Huaihe River
17 Basin, School of Geography and Tourism, Anhui Normal University, Wuhu 241000, China;

18 ⁵School of Resources and Environment, University of Electronic Science and Technology of China,
19 Chengdu 611731, China

20 ⁶Institute of Urban Study, School of Environmental and Geographical Sciences (SEGS), Shanghai
21 Normal University, Shanghai 200234, China

22 ⁷Hebei Technology Innovation Centre for Remote Sensing Identification of Environmental Change,
23 Hebei Key Laboratory of Environmental Change and Ecological Construction, School of
24 Geographical Sciences, Hebei Normal University, Shijiazhuang 050024, China

29 **Abstract:**

30 Oases and deserts generally act as a landscape matrix and mosaic in arid/semiarid
31 regions. The significant difference of thermal and dynamic characteristics between
32 oasis and desert surface will result in oasis-desert interaction. That is, the interaction
33 between oasis and desert system through the exchange of momentum, energy, water
34 and carbon, which can lead to a series of microclimate effects that affect the structure
35 of the atmospheric boundary layer, changes of carbon sources/sinks in oasis and the
36 local ecological environment. Therefore, studying water, heat and carbon exchange is
37 significant for achieving the goals of carbon peaking and carbon neutrality in oasis-
38 desert areas and supporting the ecological security and sustainable development of
39 oases. To monitor energy, water vapor and carbon exchange between the land surface
40 and atmosphere, a land surface process integrated observatory was established in the
41 oasis-desert area in the middle and lower reaches of the Heihe River Basin, the 2nd
42 largest endorheic basin in China. In this study, we present a suite of observational
43 datasets in artificial and natural oases-desert systems, which consist of long-term energy,
44 water vapor, carbon/methane fluxes, and auxiliary data involving hydrometeorology,
45 vegetation and soil parameters from 2012 to 2021. Half-hourly turbulent flux data were
46 acquired by an eddy covariance system and scintillometer. The hydrometeorological
47 data, including radiation, soil heat flux and soil temperature profile, gradient of air
48 temperature/humidity and wind speed/direction, air pressure, precipitation and soil
49 moisture profiles, were observed from automatic weather stations with a 10-minute
50 average period as well as the groundwater table data. Moreover, vegetation and soil

51 parameters were also supplemented in the datasets. Careful data processing and quality
52 control are implemented during data production, including data collection, processing,
53 archiving and sharing. The current datasets can be used to explore the water-heat-carbon
54 process and its influence mechanism, calibrate and validate related remote sensing
55 products, simulate energy, water vapor and carbon exchange in oasis and desert areas,
56 and provide references and representatives for other similar artificial and natural oases
57 along the Silk Road. The datasets are available from the National Tibetan Plateau Third
58 Pole Environment.

59

60 **1. Introduction**

61 Arid and semiarid regions represent approximately 30% of the global terrestrial surface
62 area (Dregne, 1991; Scanlon et al., 2006), and dryland expansion occurs under climate
63 change, especially in developing countries (Huang et al., 2015). This proportion is much
64 higher in China, as (semi)arid regions account for approximately 47% of its terrestrial
65 surface (Zhang et al., 2016a; Mao et al., 2018). An oasis is a unique ecological
66 landscape in arid and semiarid areas, which is not only the core of its ecological
67 environment but also the foundation of its economic development, especially in western
68 China, which has been an important part of the ‘Silk Road’ since ancient times. Oases
69 with less than 10% of the total area of arid regions support more than 90% of the
70 population in the arid regions of China (Chu et al., 2005; Li et al., 2016; Zhou et al.,
71 2022). The main geomorphologic feature is a wide sandy desert or Gobi (gravel desert),
72 interspersed with many oases of different sizes and shapes in the middle and lower

73 reaches of a typical endorheic basin in Northwest China (Cheng et al., 1999). The water
74 from upstream is the link connecting these ecosystems, and the oasis is the place where
75 human beings live. The oasis areas are now 3.3 times larger than those in the early
76 1950s in the region of northwestern China (Zhang et al., 2018). The oasis-desert system
77 plays a crucial role in maintaining a stable ecological environment and agricultural
78 productivity (Zhang and Zhao, 2015). However, inland river basins in arid and semiarid
79 areas are facing the crisis of ecological environment degradation, such as the drying up
80 of rivers and lakes, the degradation of natural vegetation, the intensification of land
81 desertification and the frequent occurrence of dust storms, especially in many inland
82 river basins westward along the Silk Road, such as the Tarim River Basin (Zhao et al.,
83 2013), Aral Sea Basin (Stanev et al., 2004; Crétaux et al., 2009), and Lake Urmia Basin
84 (Stone, 2015). Therefore, it is critical to maintain the balance between the oasis and
85 desert systems to achieve the goal of sustainable oasis development.

86 The particularity of the underlying surface in the oasis-desert area, e.g., the irrigation
87 cropland, riparian forest, sandy vegetation, seasonal snow and frozen soil, makes the
88 study of land-atmosphere interactions complex and needs comprehensive consideration
89 in such heterogeneous underlying surfaces. The dynamic and thermal characteristics of
90 the underlying surface of the oasis and the desert are significantly different, and the
91 oasis and desert systems interact and influence each other through momentum, energy,
92 water vapor and carbon exchange. Thus, the oasis-desert interaction will affect the
93 structure of the atmospheric boundary layer and the local ecological environment.
94 Additionally, under the influence of weather conditions, the oasis-desert interaction

95 results in the local circulation between oasis and desert and airflows form dynamic and
96 thermal inner boundary layer within the oasis (Cheng et al., 2014). These can lead to
97 the local microclimate characteristics of the oasis-desert area (Liu et al., 2020), such as
98 the wind shield effect and cold-wet island effect of the oasis, the humidity inversion
99 effect within the surrounding desert, and oasis carbon sources/sinks. These
100 microclimate effects play an important role in the self-sustaining and development of
101 oasis systems. Understanding the basic characteristics of energy, water vapor and
102 carbon exchange in oasis-desert ecosystems is important for achieving the goals of
103 carbon peaking and carbon neutrality in the oasis-desert area and supporting ecological
104 security and sustainable development of the oasis.

105 Extensive studies have investigated energy, water vapor and carbon exchange in
106 oasis-desert areas based on field and remote sensing observations (Taha et al., 1991;
107 Potchter et al., 2008; Xue et al., 2019; Wang et al., 2019; Zhou et al., 2022) and
108 numerical simulations (Chu et al., 2005; Meng et al., 2009; Georgescu et al., 2011; Liu
109 et al., 2020). Li et al. (2016) provided a complete sketch map of oasis and desert
110 interactions based on previous studies, including the oasis cold and wet island effect,
111 oasis wind shield effect (oasis effect), and air humidity inversion effect within the
112 surrounding desert (desert effect), which are important for the stability and
113 sustainability of the oasis-desert ecosystem (Liu et al., 2020). In addition, the oasis-
114 desert areas located in semiarid regions were found to be carbon sinks by previous
115 researchers (Tagesson et al., 2016; Wang et al., 2019), which can significantly affect
116 the carbon balance of arid regions and play an increasingly important role within the

117 global carbon cycle.

118 The Heihe River Basin (HRB), the second largest endorheic basin in China, is
119 characterized by artificial oases and natural oases in the middle and lower reaches,
120 respectively. Several experiments have been conducted in these oasis-desert areas, e.g.,
121 the Heihe River Basin Field Experiment (HEIFE) from 1990 to 1992 to conduct
122 comprehensive studies of atmosphere–land surface interactions over the Zhangye oasis
123 and desert area in the middle reaches of the HRB (Wang et al., 1992), the Jinta
124 experiment from 2005 and 2008 to focus on the energy and water exchange and the
125 atmospheric boundary over the Jinta oasis and desert area in the middle reaches of the
126 HRB (Wen et al., 2012), the oasis-desert area in the middle reaches and mountainous
127 area in upper reaches of watershed allied telemetry experimental research (WATER)
128 and the subsequent HiWATER (oasis-desert area in the middle and lower reaches and
129 mountainous area in upper reaches) to be a comprehensive simultaneous satellite–
130 airborne–ground observations eco-hydrological experiment (Li et al., 2009, 2013).
131 Thereafter, a multielement, multiscale, networked, and elaborate integrated observatory
132 network was established in the oasis-desert area in the middle and lower reaches and
133 mountainous area in upper reaches of the HRB since 2007 and completed in 2013 (Liu
134 et al., 2018). A quantitative understanding of the energy, water vapor and carbon
135 exchange in oasis-desert areas is crucial for recognizing the oasis-desert interactions
136 and is significant for protecting the ecological stability and socioeconomic development
137 of oases, and long-term observations are indispensable. The observations and research
138 findings from the oasis-desert area in the HRB will serve as references and

139 representatives for other similar artificial and natural oases along the Silk Road. To
140 achieve the aforementioned objective, observations should be continuously conducted,
141 and a high-quality dataset should be obtained.

142 In this paper, the integrated observatory network of the artificial and natural oasis-
143 desert areas in the middle and lower reaches in the HRB are introduced first, and the
144 observations characterizing the energy, water vapor and carbon exchange are detailed
145 explicated, which provides a 10-year dataset. Specifically, the spatial distribution and
146 design of the observation sites are summarized in Section 2. Section 3 describes the
147 data processing and quality control procedures. In Section 4, the energy, water vapor
148 and carbon fluxes and related auxiliary parameters are introduced in detail. The data
149 availability is documented in Section 5, and the conclusions are summarized in Section
150 6. This dataset can be used for comprehensive understanding of energy, water vapor
151 and carbon exchange in oasis-desert areas, and validating simulation results and remote
152 sensing products of energy, water vapor and carbon fluxes in oasis-desert areas.

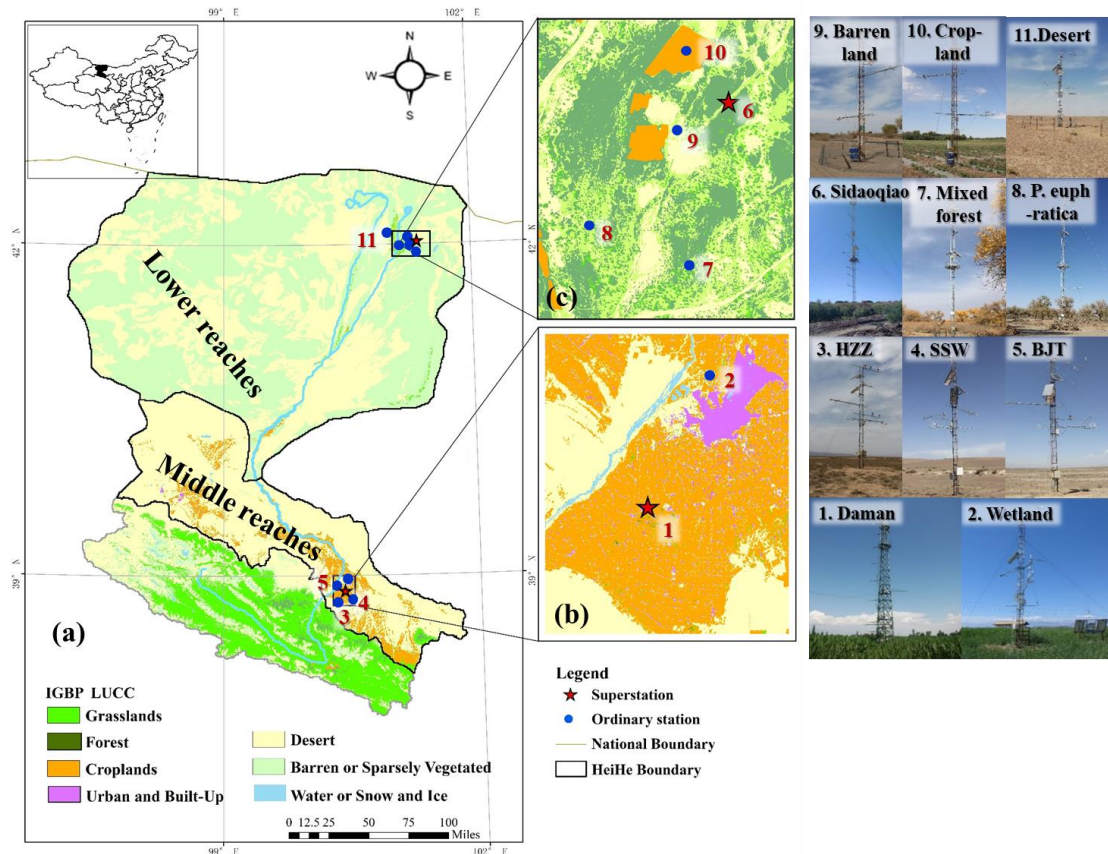
153 **2. A land surface process integrated observatory network in the oasis-desert area** 154 **of the HRB**

155 **2.1 Study area description**

156 The study areas are the middle and lower reaches of the HRB, which are located in
157 the arid regions of western China, provided by water from the typical cryosphere of the
158 upper reaches. In the upper reaches, glaciers, snow cover and frozen ground is widely
159 distributed and snowfall could occur in any season (elevation >3800 m). The typical

160 snow depth is 15-30 cm with a duration of 90-120 days in the snow-covered regions
161 (Che et al., 2012; Che et al., 2019). The middle reaches, typical of the artificial oasis-
162 desert system in Zhangye City, the largest oasis in the Hexi Corridor, cover an area of
163 29,717 km² with an oasis area of 5,560 km², while the lower reaches in Ejina Banner
164 have a natural oasis-desert system covering an area of 85,678 km² with an oasis area of
165 1,130 km² (Fig. 1). Among the oases, agricultural oases can be traced to the history of
166 more than 2000 years. The annual average air temperature was 7.29 °C and 9.75 °C,
167 and the annual accumulated precipitation was 184.83 mm and 37.31 mm (1979-2018)
168 in the middle and lower reaches, respectively.

169 Eleven land surface fluxes and meteorological stations have been established in these
170 regions since 2012 with two superstations and eleven ordinary stations (Table 1; Section
171 2.2), specifically two oasis stations and three desert stations in the middle reaches and
172 five oasis stations and one desert station in the lower reaches.



173

174 Fig. 1. The middle and lower reach observation systems in the HRB. (a: Heihe River

175 basin; b: Stations in the Zhangye artificial oasis-desert area in the middle reaches; c:

176 Stations in the Ejina natural oasis area in the lower reaches)

177

Table 1. Station information in the middle and lower reaches of the HRB

ID	Name	Longitude (°, E)	Latitude (°, N)	Elevation (m)	Land Cover	Duration	Location
1	Daman	100.37	38.86	1556	Maize	May 2012- present	Oasis in midstream, superstation
2	Zhangye Wetland	100.45	38.98	1460	Wetland mainly reed	June 2012- present	Oasis in midstream, ordinary station
3	Huazhaizi Desert Steppe	100.32	38.77	1731	<i>Kalidium foliatum</i>	June 2012- present	Desert in midstream, ordinary station
4	Shenshawo Sandy Desert	100.49	38.79	1594	Sandy	June 2012- Apr.2015	Desert in midstream, ordinary station
5	Bajitan Gobi	100.30	38.92	1562	Reaumuria	May 2012- Apr.2015	Desert in midstream, ordinary station
6	Sidaoqiao	101.14	42.00	873	<i>Tamarix</i>	July 2013-	Oasis in downstream,

						present	superstation
7	Mixed Forest	101.13	41.99	874	<i>Populus euphratica and Tamarix</i>	July 2013-present	Oasis in downstream, ordinary station
8	Populus euphratica	101.12	41.99	876	<i>Populus euphratica</i>	July 2013-Apr.2016	Oasis in downstream, ordinary station
9	Barren Land	101.13	42.00	875	Bare land	July 2013-Mar.2016	Oasis in downstream, ordinary station
10	Cropland	101.13	42.00	875	Melon	July 2013-Nov.2015	Oasis in downstream, ordinary station
11	Desert	100.99	42.11	1054	Reaumuria	Apr.2015-present	Desert in downstream, ordinary station

178 2.2 Observation systems

179 2.2.1 Artificial oasis and desert areas in the middle reaches

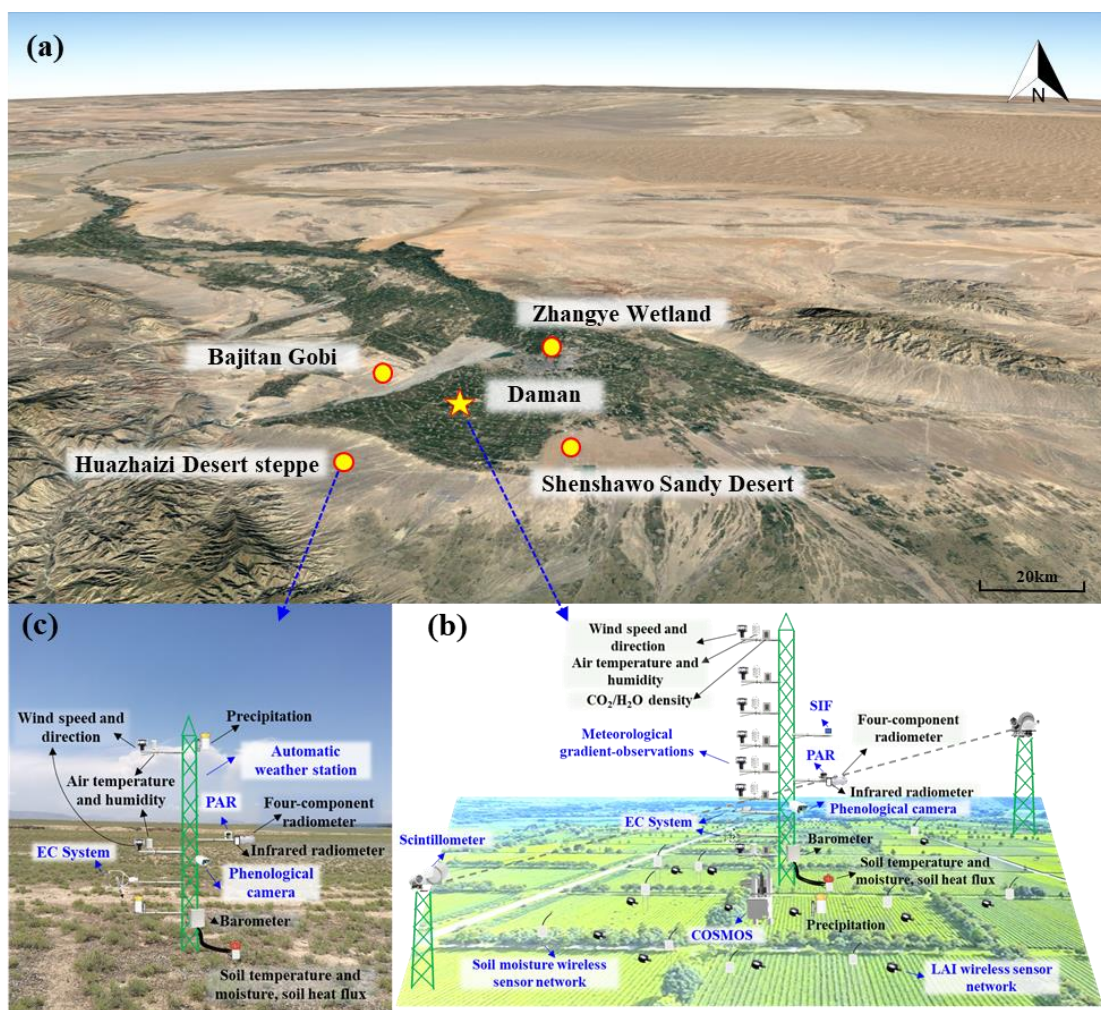
180 The middle reaches are located in the Zhangye oasis in Zhangye City of Gansu
181 Province, and the primary underlying surfaces include cropland (maize), shelterbelt,
182 orchard, residential area and wetland (reed) in the oasis and sandy desert, desert steppe
183 (*Kalidium foliatum*), and the Gobi Desert (Reaumuria) in the surrounding desert. Five
184 stations (one superstation and four ordinary stations) were established in these surfaces,
185 which are representative of the main underlying surface types within the oasis-desert
186 area in the middle reaches of the HRB.

187 There is one superstation (maize and shelterbelt) and one ordinary station (wetland
188 and reed) in the Zhangye oasis surrounding three ordinary stations in the desert located
189 in the middle reaches of the HRB (Fig. 2a). The superstation includes a multiscale
190 observation system for energy, water vapor and carbon fluxes (lysimeter-EC system-
191 scintillometer for meter-hundred-kilometer observation scale) and soil moisture

192 measurements (*in situ* soil moisture profile-cosmic ray probe-soil moisture wireless
193 sensor network for meter-hundred-kilometer observation scale), and it includes a
194 hydrometeorological gradient observation system to monitor the profile (7 layers) of
195 wind speed/direction, air temperature/humidity and carbon dioxide and water vapor
196 concentration, one layer four-component radiation, air pressure, precipitation, and
197 infrared temperature (2 repetitions), 9/8 layers' soil temperature/moisture profile, soil
198 heat flux (3 plates with two buried under the bare soil between two corn plants and one
199 buried under the corn plants), etc. The EC and hydrometeorological gradient
200 observation system were installed on a 40 m tower. Optical and microwave
201 scintillometers were installed on both sides of the 40 m tower apart from 1854 m. There
202 were also observations of vegetation parameters in the 40 m tower, including a visible
203 and near infrared phenological camera to monitor the vegetation index and crop growth
204 curve, two photosynthetically active radiation (PAR) sensors to monitor PAR, a
205 vegetation chlorophyll fluorescence observation system to monitor sun-induced
206 chlorophyll fluorescence (SIF), and an LAI wireless sensor network (28 nodes) to
207 monitor multipoint LAI in the source area of the scintillometer (Fig. 2b, Fig. 4a).

208 The ordinary stations are comprised of an EC system, an automatic weather station
209 (AWS) and a visible and near infrared phenological camera. The observation elements
210 of the AWS include two layers' air temperature/humidity and wind speed/direction, one
211 layer's four-component radiation, air pressure, and infrared temperature (2 repetitions),
212 two layers' precipitation, 8/7 layers' soil temperature/moisture, soil heat flux (3 plates),
213 etc. (Fig. 2c).

214 The sonic anemometers of the ECs were installed at a height of approximately 3-7 m
 215 above the canopy to capture the sensible heat, latent heat, carbon dioxide and methane
 216 (in wetland) fluxes, etc. The sonic anemometers of all the ECs were aimed toward the
 217 north. Soil parameters, such as soil texture, porosity, bulk density, saturated hydraulic
 218 conductivity, and soil organic matter content, etc. were investigated at each station in
 219 2012 and 2020. Detailed information can be found in Table 2.



220
 221 Fig. 2. Sketch map of the artificial oasis and desert area in the middle reaches (a:
 222 artificial oasis and desert area (from © Google Earth); b: Daman superstation; c:
 223 Huazhaizi ordinary station)

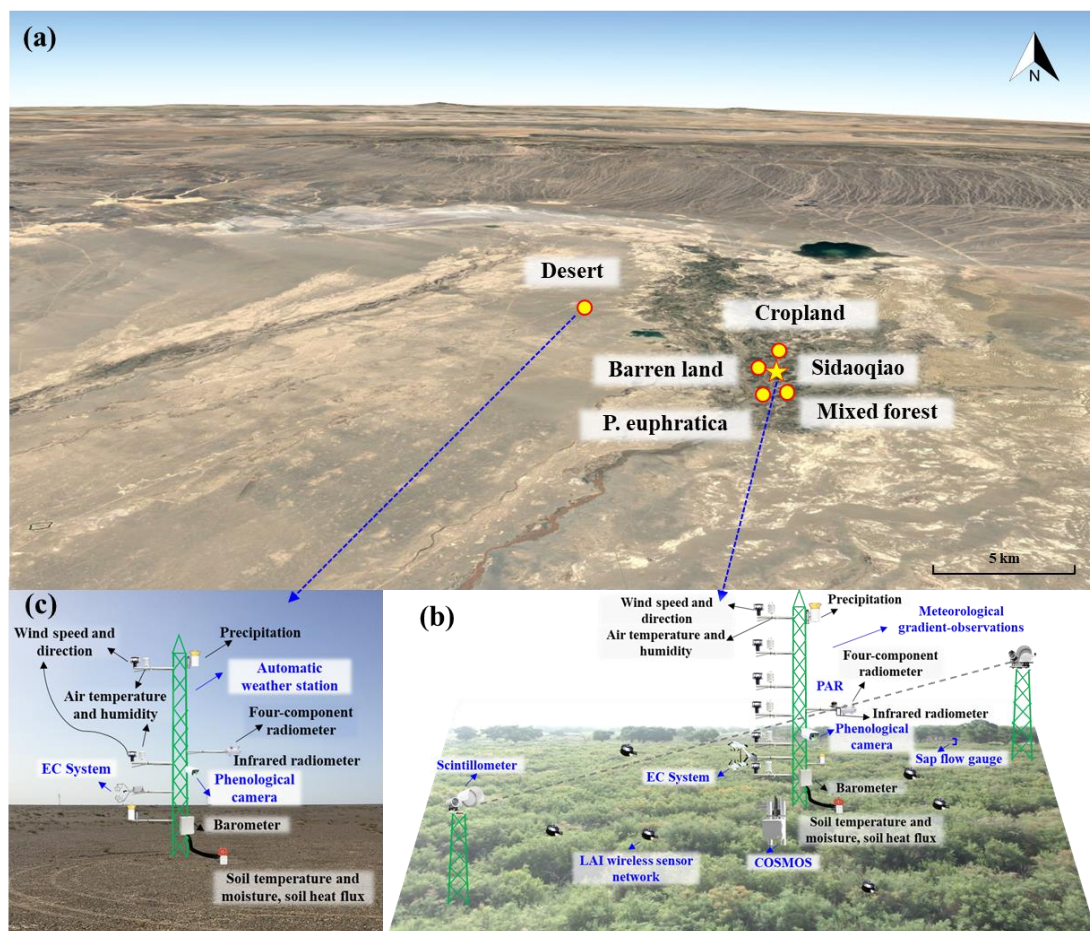
224 2.2.2 Natural oasis and desert areas in the lower reaches

225 The Ejin Banner oasis is located in the lower reaches of the HRB and belongs to
226 Inner Mongolia and part of Jiuquan city of Gansu Province, which is surrounded by
227 widespread desert. The main underlying surfaces were Reaumuria and terminal lake in
228 desert, riparian forest, cropland, barren land and residential area in the oasis in the lower
229 reaches. There were six stations (one superstation and five ordinary stations) in the
230 lower reaches, which are located in these land covers, including *Populus euphratica*,
231 *Tamarix chinensis*, cropland, barren land, and desert.

232 In the oasis-desert area of the lower reaches, there is one superstation and four
233 ordinary stations in the oasis and one ordinary station in the desert (Fig. 3a). The
234 superstations include a multiscale observation system for energy, water vapor and
235 carbon fluxes (sap flow gauge-EC-large aperture scintillometer for meter-hundred-
236 kilometer observation scale) and soil moisture measurements (*in situ* soil moisture
237 profile and cosmic ray probe for meter and hundred meter observation scale), a
238 hydrometeorological gradient observation system to monitor the profile (6 layers) of
239 wind speed/direction, air temperature/humidity, one layer four-component radiation, air
240 pressure, and infrared temperature (2 repetitions), two layers of precipitation, 10/9
241 layers soil temperature/moisture profile, soil heat flux (with two buried under the bare
242 soil and one buried under the *Tamarix* plants), etc. The EC and hydrometeorological
243 gradient observation system were installed on a 28 m tower. Two groups of large
244 aperture scintillometers were installed on both sides of the 28 m tower apart from 2350
245 m. The vegetation parameter observations included PAR and the phenological camera

246 to monitor the vegetation index and crop growth curve installed in the 28 m tower and
 247 LAI wireless sensor network (11 nodes in the source area of the scintillometer) (Fig. 3b,
 248 Fig. 4b). The ordinary stations are comprised of an EC system, an AWS and a visible
 249 and near infrared phenological camera. (Fig. 3c).

250 Additionally, thermal infrared radiometers and imagers were installed at the Mixed
 251 Forest and Sidaoqiao stations to measure different component temperatures, i.e., the
 252 brightness temperature of different land cover types under different illumination
 253 conditions (Li et al., 2019). The soil parameters and groundwater table were observed
 254 around the stations. Detailed information can be found in Table 2.



255
 256 Fig. 3 Sketch map of the natural oasis and desert areas in the lower reaches (a: natural
 257 oasis and desert area (from © Google Earth); b: Sidaoqiao superstation; c: desert

258 ordinary station)

259 Table 2 Observation variables and sensor configurations of surface flux,
 260 hydrometeorology, vegetation and soil parameters

Observations	Sensor	Manufactory	Height/depth (m)	Sites
<i>Surface flux observations:</i>				
Sensible heat, latent heat, carbon dioxide, methane flux	CSAT3&Gill, Li7500&Li7500 A&Li7500DS& EC155&Li7700 CPEC310	Campbell and LiCor, USA	3~7 m above the canopy	All stations (methane observation only in wetland, closed path EC at Daman and Desert, stations)
Sensible and latent heat flux	BLS900 and MWSC-160	Scintec and RPG, Germany	23.92	Daman
	BLS900	Germany	25.5	Sidaoqiao
Sap flow	TDP 30	Rainroot, China	1.5	Mixed forest
<i>Hydrometeorological observations:</i>				
Pressure	PTB110	Vaisala, Finland	--	Bajitan, Shenshawo
	AV-410BP	Avalon, USA	--	Mixed Forest
	PTB210	Vaisala, Finland	--	Huazhaizi
	CS100	Campbell, USA	--	Daman, Wetland, Sidaoqiao, Desert
Precipitation	TE525MM	Texas Electronics, USA	--	Daman, Wetland, Huazhaizi, Bajitan, Shenshawo,Sidaoqiao, Desert
	52203	RM Young, USA	--	Mixed Forest
Wind speed/direction	Windsonic	Gill, UK	3,5,10,15,20,30,40 5,7,10,15,20,28	Daman, Sidaoqiao
			5,10	Wetland, Huazhaizi, Mixed forest
	010C/020C	Met One	5,10	Wetland, Desert
	03001	RM Young, USA	10 28	Bajitan,Shenshawo Populus euphratica
Air temperature/hu	HMP45D	Vaisala, Finland	28	Mixed Forest

midity	HC2S3	Vaisala, Finland	5,7,10,15,20,28	Sidaoqiao
	HMP45AC	Vaisala, Finland	5,10	Bajitan,Huazhaizi, Shenshawo,Wetland, Desert
			28	Populus euphratica
AV-14TH	Avalon	3,5,10,15,20,30,40	Daman	
Four- component radiation	CNR4	Kipp&Zonen, Netherland	10	Sidaoqiao
			22	Mixed Forest
	CNR1	Kipp&Zonen, Netherland	6	Wetland,Huazhaizi,Bajita n,Shenshawo,Desert,Barr en land, Cropland
			22	Populus euphratica
PSP&PIR	Eppley, USA	12	Daman	
Infrared temperature	SI-111	Apogee, USA	12	Daman
			10	Sidaoqiao
			22	Populus euphratica, Mixed Forest
			6	Wetland,Huazhaizi,Bajita n,Shenshawo,Desert,Barr en land, Cropland
Soil temperature profile	109ss-L	Campbell, USA	0,-0.02,-0.04,-0.1,- 0.2,-0.4,-0.8,-1.2,-1.6,- 2.0	Sidaoqiao, Desert Wetland
			0, -0.02,-0.04,-0.1,- 0.2,-0.4,-0.6,-1.0	
	AV-10T	Avalon, USA	0, -0.02,-0.04,-0.1,- 0.2,-0.4,-0.6,-0.8,-1.2,- 1.6	Daman
			0, -0.02,-0.04,-0.1,- 0.2,-0.4,-0.6,-1.0	Bajitan, Huazhaizi
			0, -0.02,-0.04,-0.1,- 0.2,-0.4	Wetland
			0,-0.02,-0.04,-0.1,- 0.2,-0.4,-0.6,-1.0,-1.6,- 2.0,-2.4	Mixed forest
	109	Campbell, USA	0, -0.02,-0.04,-0.1,- 0.2,-0.4,-0.6,-1.0	Shenshawo
			0, -0.02,-0.04	Barren land, Cropland, Populus euphratica

Soil moisture profile	ECH ₂ O-5	Decagon Devices, USA	-0.02,-0.04,-0.1,-0.2,-0.4,-0.6,-1.0	Bajitan
	CS616	Campbell, USA	-0.02,-0.04,-0.1,-0.2,-0.4,-0.6,-0.8,-1.2,-1.6	Shenshawo, Desert
	ML2X	Delta-T, UK	-0.02,-0.04,-0.1,-0.2,-0.4,-0.8,-1.2,-1.6,-2.0	Daman
			-0.02,-0.04,-0.1,-0.2,-0.4,-0.6,-1.0,-1.6,-2.0,-2.4	Sidaoqiao
				Mixed Forest
				Barren land, Populus euphratica, Cropland
	ML3	Delta-T, UK	-0.02,-0.04,-0.1,-0.2,-0.4,-0.6,-1.0	Desert, Huazhaizi
Soil heat flux	HFP01	Hukseflux, Netherland		Wetland,Huazhaizi, Bajitan,Shenshawo,Desert,Barren land, Cropland
	HFT3	Campbell, USA	-0.06	Bajitan, Populus euphratica, Mixed forest
	HFP01SC	Hukseflux, Netherland		Daman, Sidaoqiao
Averaged temperature	TCAV	Campbell, USA	-0.02, -0.04	Daman, Sidaoqiao
CO ₂ /H ₂ O profile	AP200	Campbell, USA	3,5,10,15,20,30,40	Daman
Groundwater Table	U20	Onset, USA	-2~-3m	Sidaoqiao, Mixed forest, Populus euphratica, Cropland, Desert
<i>Vegetation parameter observations:</i>				
Vegetation phenology	Phenological camera	XST-PhotoNet, China	above the canopy	All sites
LAI	XST-LAINet	Beijing StarViewer Science and Technology Ltd., China	Below the canopy	28 nodes around Daman, 6 nodes around Sidaoqiao, 5 nodes around Mixed forest
photosynthetically active radiation	PQS-1	Kipp&Zonen, Netherland	0.5, 12	Daman
			10	Sidaoqiao
			22	Mixed forest, Populus euphratica
			6	Wetland, Cropland

		Beijing		
Sun-induced		Bergsun		
chlorophyll	AutoSIF-1	Spectral	34	Daman
fluorescence		Technology		
		Co. Ltd, China		

Soil parameters: soil sampling and laboratory testing in 2012 and 2020

261

262 **3. Data processing and quality control**

263 The data processing and quality control procedure can be divided into data collection,
 264 data processing and data archiving and sharing (Fig. 4).

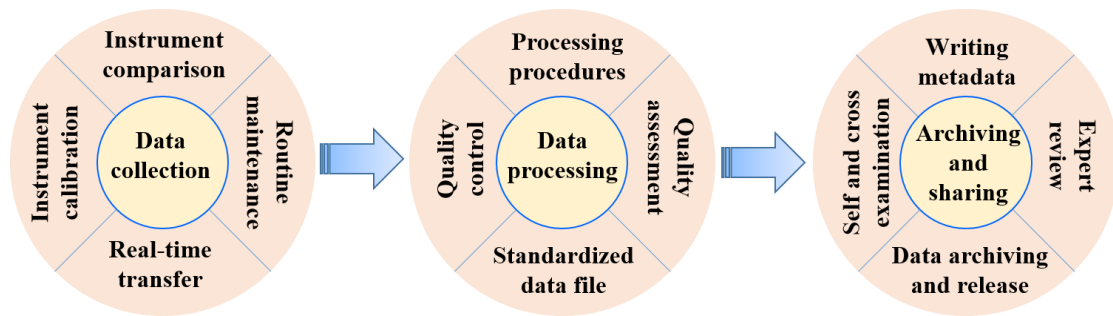
265 In the data collection step, the comparison and calibration of instruments are
 266 prerequisites to ensure the quality of the observation data. The instrument comparison
 267 experiments were specifically arranged under the Gobi Desert in 2012 in the middle
 268 reaches (Xu et al., 2013) and shrub in 2013 in the lower reaches (Li et al., 2018) to
 269 ensure the consistency and comparability of the instruments. In addition, the
 270 instruments with multiple layers were compared at the same height before installation,
 271 the soil moisture probes were also compared under dry and wet conditions, and the
 272 multitype rain gauges were compared in the same field. The infrared gas analyzer of all
 273 the EC systems was calibrated at the beginning and end of the vegetation-growing
 274 season every year. To ensure the data quality, a routine maintenance procedure is
 275 formulated and strictly followed, including daily (checking the real-time data through
 276 remote monitoring and data management system for field observatory network v1.0),
 277 10 days (checking the time series plot providing by the system), monthly (routine
 278 inspection in every station), and annually (data processing and release) (Liu et al., 2018).
 279 The Heihe watershed internet of things observation system was developed to complete

280 the above maintenance procedure, which included remote receiving and storing the filed
281 data, browsing and processing real-time data, monitoring the instrument status and early
282 warning the abnormal conditions, etc.

283 During the data processing step, a processing scheme was formulated for each type
284 of instrument. For the EC system, the data were processed from the raw 10 Hz turbulent
285 data, including spike detection, sonic temperature correction, coordinate rotation,
286 frequency response correction, and WPL (Webb-Pearman-Leuning) correction. (Liu et
287 al., 2016; Wu et al., 2023). Additionally, the 30-min flux data series were identified as
288 quality flags according to the stationarity test and integral turbulence characteristics test.
289 A final quality flag (1~9) was assigned to each specific turbulent flux value, indicating
290 good quality (1~3), suitability for general use (4~6), poor but better than gap filling data
291 (7~8), and discarded data (9). The unclosed energy balance of EC system is a universal
292 problem. There was approximately an average of 17% energy imbalance in our study
293 area (Xu et al., 2017; Zhou et al., 2018), which was reasonable compared with previous
294 results (Stoy et al., 2013). The Bowen-ratio correction method is recommended to close
295 the energy balance (Twine et al., 2000; Xu et al., 2020). The data processing steps from
296 scintillometer measurements to surface fluxes are as follows: raw data to light intensity
297 variance, light intensity variance to the structure parameter of the refractive index of air
298 (C_n^2), C_n^2 to meteorological data, and finally obtaining surface fluxes combining the
299 meteorological data. Four steps are taken to ensure the quality of scintillometer data
300 (Liu et al. 2011; Zheng et al., 2023): (i) excluding data for C_n^2 beyond the saturation
301 criterion; (ii) excluding data obtained during periods of precipitation; (iii) excluding

302 data when the demodulated signal is small; and (iv) excluding data when the sensor is
303 malfunctioning. The steps of the meteorological gradient observation system and AWS
304 data processing and quality control were twofold: (1) all the AWS data were averaged
305 over an interval of 10 min for a total of 144 records per day. The missing data were
306 denoted by -6999; (2) the unphysical data were rejected, and the gaps were denoted by
307 -6999. The surface soil heat flux was calculated using the ‘PlateCal’ approach
308 (Liebethal et al., 2005), and the final surface soil heat flux was the weighted vegetation
309 fraction combined with the soil temperature and moisture measured above the heat
310 plates. There are approximately 10–20% missing or rejected values of EC or
311 scintillometer data. The look-up table (LUT) method is recommended to fill the gaps
312 when data were missing (Xu et al., 2020). The maximum missing values of AWS data
313 were no more than 10%, and linear interpolation method is recommended to fill the
314 missing values. The vegetation growth curve and vegetation index can be obtained from
315 visible and near infrared bands measured by phenological cameras. The key
316 phenological parameters are determined according to growth curve fitting, such as the
317 growth season start date, peak, and growth season end. The leaf area index (LAI) data
318 were obtained from the LAINet sensor, which can continuously measure the multipoint
319 total solar radiation above the canopy and the transmitted radiation below the canopy,
320 and the LAI was calculated based on multiangle transmittance data (Qu et al., 2014).
321 Seven days moving averaged method is recommend to eliminate noise from the daily
322 LAI observations (Qu et al., 2014). Then, all the data are processed into a standardized
323 file for sharing.

324 During the archiving and sharing step, the metadata were written for each data point,
 325 including the site description, processing step, header description, and other notes. (Li
 326 et al., 2017a). Before data are released, self-examination, crosschecks and expert review
 327 are required to ensure data quality. Finally, the data were archived and shared online.



328

329 Fig. 4 Flowchart of data processing and quality control

330 4. Data description

331 4.1 Energy, water vapor and carbon fluxes data

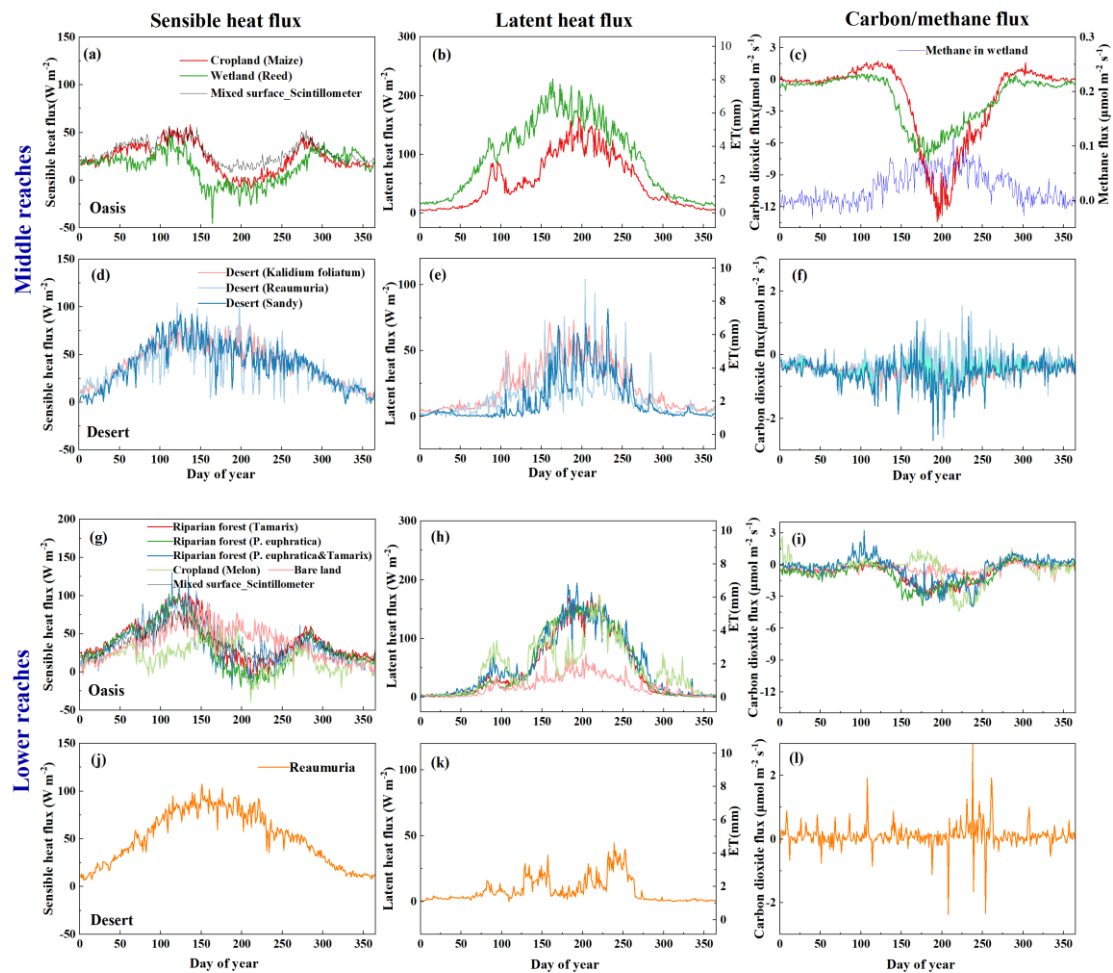
332 The EC systems were used to measure surface flux at all sites, namely, 5 stations (2
 333 in oasis, 3 in desert) in the middle reaches and 6 stations (5 in oasis, 1 in desert) in the
 334 lower reaches. The turbulent flux data were recorded by the open path or closed path
 335 EC systems and processed carefully. In addition to the surface flux of sensible, latent
 336 and carbon dioxide, the methane flux was also observed at the wetland site in the middle
 337 reaches (Table 2). The multiyear seasonal variations in sensible heat, latent heat, carbon
 338 dioxide and methane fluxes are shown in Figure 5. Generally, the latent heat fluxes in
 339 oases are obviously higher than those in deserts, especially in the lower reaches. The
 340 latent heat fluxes exhibited a single peak during one year, with a peak value of
 341 approximately 200 W m^{-2} in the oasis area; however, they significantly fluctuated due
 342 to irrigation (normally 4 times in cropland of the midstream region, 2 times in riparian
 343 forest and melon of the downstream region) or precipitation. In the middle reaches, the
 344 latent heat flux in the wetland showed the largest values, which were more than 200 W

345 m^{-2} in the crop growing season, and it also presented relatively large values in the
346 midstream piedmont desert region with dense *Kalidium foliatum* cover (peak value
347 greater than 50 W m^{-2}). In the lower reaches, the latent heat flux showed consistent
348 variations in the riparian forest with a peak value of approximately 150 W m^{-2} during
349 the crop growing season; however, it showed large fluctuations in the melon surface
350 during growth due to frequent irrigation (approximately 7~8 times), and the bare land
351 in the oasis and desert had a small latent heat flux.

352 The seasonal variations in sensible heat flux were totally different in the oasis and
353 desert systems. The sensible heat flux showed two peaks in the oasis in both the middle
354 and lower reaches except for the bare land, namely, reaching maximum values at the
355 end of April and September, and it showed minimum values in mid-August (-25 W m^{-2}),
356 corresponding to large values of latent heat flux in the oasis that were even greater
357 than net radiation. This phenomenon was also found by previous researchers (Liu et al.,
358 2011) and was called the ‘oasis effect’. In the desert area, the sensible heat flux appeared
359 as a single peak in spring and decreased gradually since then. The variation in sensible
360 heat flux in bare land of the natural oasis in the lower reaches is similar to that in the
361 desert area.

362 In the oasis, the carbon dioxide (CO_2) flux showed obvious ‘U’ variations, especially
363 in the middle reaches. The crop absorbed carbon dioxide (carbon sink) in the crop-
364 growing season, and a negative value of approximately $-14 \mu\text{mol m}^{-2} \text{ s}^{-1}$ was observed
365 in the maize surfaces. The magnitude of the methane (CH_4) flux was lower than the
366 CO_2 flux and was in the range of approximately $0\sim 0.1 \mu\text{mol m}^{-2} \text{ s}^{-1}$ in the wetland. The
367 CH_4 flux in the non-growing season was the lowest and increased rapidly in April.
368 Although the magnitude of the CH_4 flux was lower than the CO_2 flux, the contribution

369 of methane emissions to global warming was as important as CO₂ contributions on a
 370 long time scale (Hommeltenberg et al., 2014; Zhang et al., 2016b), especially focusing
 371 on CH₄ flux measurements in wetlands (Zhang et al., 2022). The variations in CO₂ flux
 372 in the riparian forest were relatively small, with values of approximately -0.4 μmol m⁻²
 373 s⁻¹ in the plant growing season. There was little carbon sequestration in the desert area
 374 due to little or sparse vegetation, and the CO₂ flux in the desert area was very small,
 375 fluctuating around zero during the years.



376
 377 Fig. 5 The multiyear seasonal variations in sensible, latent heat, carbon dioxide and
 378 methane fluxes in the oasis-desert area (sensible heat flux–left, latent sensible heat flux–
 379 middle, carbon dioxide and methane flux–right, 2012-2021)

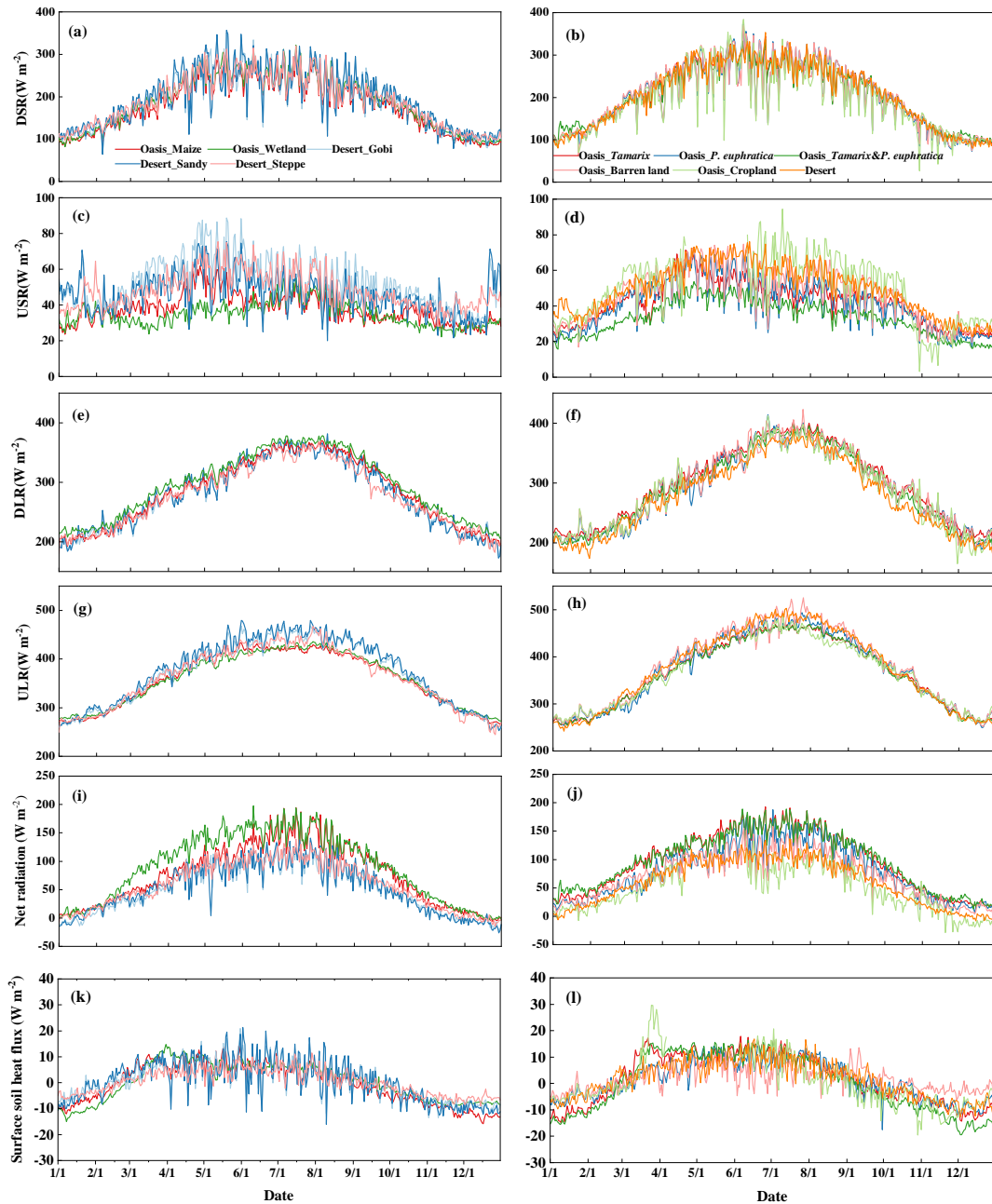
380 **4.2 Hydrometeorological data**

381 The hydrometeorological data were obtained from 13 AWSs, with six in the middle
382 reaches (Fig. 2) and seven in the lower reaches (Fig. 3) of the HRB. All the AWSs
383 recorded four-component radiations (short/long wave upward and downward radiation),
384 soil heat flux, surface and soil temperature profiles, air temperature and humidity, wind
385 speed and direction, air pressure, precipitation, soil moisture profiles, infrared
386 temperature, and groundwater table in the lower reaches. (Table 2). All sensors were
387 calibrated and intercompared before being mounted. The sampling frequencies,
388 reference heights and directions of these sensors at all stations were identical to
389 maintain consistency.

390 **4.2.1 Radiation, soil heat flux, surface and soil temperature profile**

391 It is important to understand the variations in radiation and surface soil heat flux in
392 oasis and desert areas, which are the surface available energy. Figure 6 shows the four
393 radiation components and soil heat flux in oasis and desert areas in the middle and lower
394 reaches in the HRB, and all the variables exhibited obvious seasonal variations with an
395 inverted 'U' shape. The incoming shortwave radiation was consistent with each other
396 in oasis and desert because of the short distance among the sites. Due to the higher
397 albedo in the desert, the upward shortwave radiation in the desert was larger than that
398 in the oasis (approximately larger than 30%). The incoming longwave radiation
399 originates from the atmosphere (in particular CO₂ and water vapor) and thermal
400 radiation of clouds in the lower atmosphere. The oasis presents relatively large water
401 vapor and cloudiness; thus, the incoming longwave radiation for the oasis was greater

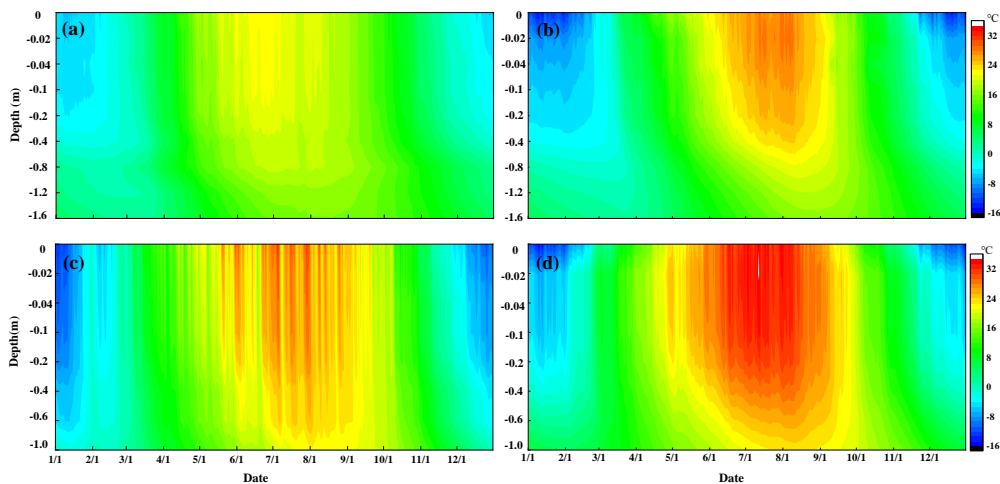
402 than that for the desert (approximately 2%). It is to be expected that under dry
403 conditions during the daytime, the surface temperature of the desert will be significantly
404 greater than that of the well-watered oasis site. Consequently, the upward longwave
405 radiation in the desert was larger than that in the oasis (approximately 8%). The net
406 radiation, driving the turbulent fluxes of sensible heat and latent heat at the earth surface
407 and heating soil, was greater in the artificial oasis and the natural oasis than in the desert
408 at approximately 50 W m^{-2} . The daily mean surface soil heat fluxes varied similarly in
409 oasis and desert areas with relatively low values in the range of -20 to 20 W m^{-2} .



410
 411 Fig. 6 Seasonal variations in multiyear average radiation components in the oasis-desert
 412 system (middle reaches: a, c, e, g, i, k; lower reaches: b, d, f, h, j, l; 2012-2021 daily
 413 averaged DSR: downward shortwave radiation; USR: upward shortwave radiation;
 414 DLR: downward longwave radiation; ULR: upward longwave radiation)

415 The soil temperature exhibited a signal peak around the year in the range of -
 416 15°C~34°C, and it decreased with increasing soil depth during the plant growing season;
 417 however, it exhibited an increasing trend in the winter. The shallow soil began to thaw

418 at the beginning of spring (march) and to freeze in autumn (November). The soil
 419 temperature changed little with depth when it exceeded 0.8 m and 1 m in the oasis and
 420 desert, respectively. The soil temperature in the desert was significantly higher by
 421 approximately 10 °C during the plant growing season than that in the oasis in both the
 422 middle and lower reaches. Additionally, the soil temperature in the artificial oasis-desert
 423 area (middle reaches) was approximately 5 °C lower during the plant growing season
 424 than that in the natural oasis-desert area (lower reaches) (Fig. 7).



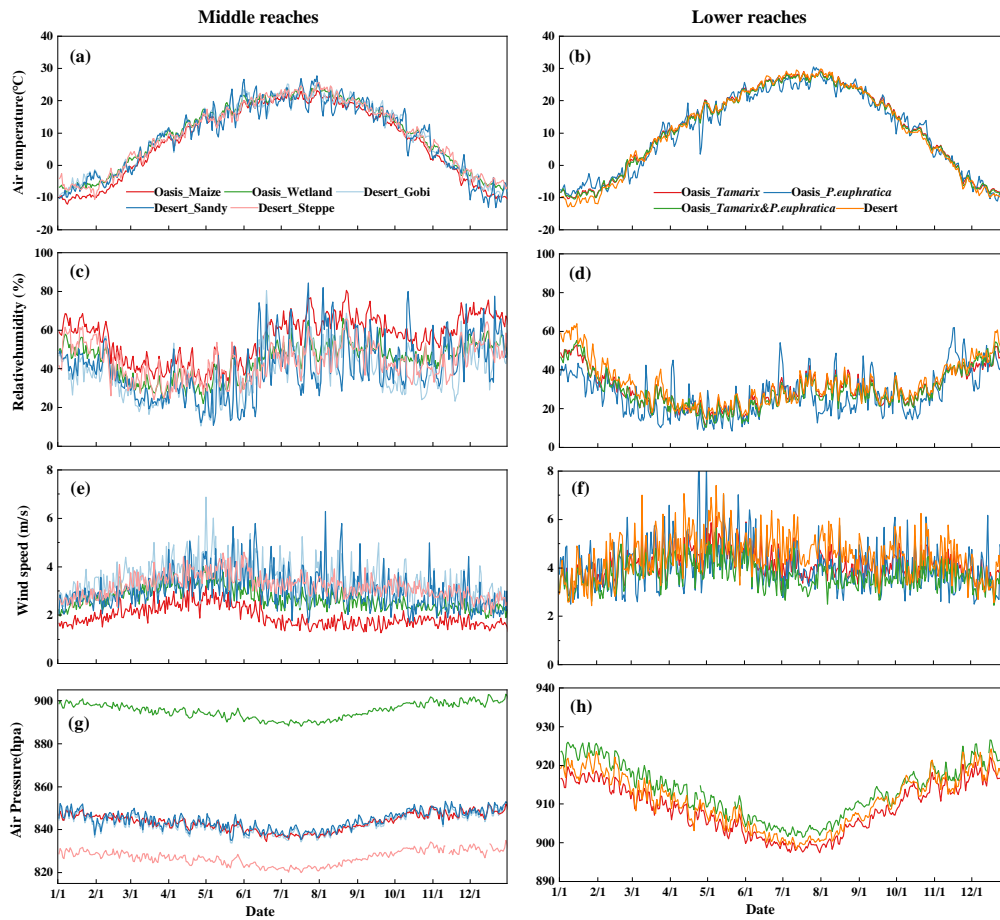
425
 426 Fig. 7. Seasonal variations in surface and soil temperature profiles in oasis and desert
 427 areas (2012-2021) (a: oasis in middle reaches–maize; b: oasis in lower reaches–*Tamarix*;
 428 c: desert in middle reaches–*Reaumuria*; d: desert in lower reaches–*Reaumuria*)

429 4.2.2 Air temperature/humidity, wind speed/direction, air pressure

430 To show micrometeorological characteristics clearly, the comparison of daily average
 431 air temperature and relative humidity (5 m except the *P. euphratica* surface with a height
 432 of 28 m), wind speed (10 m) and air pressure in desert and oasis are plotted in Figure 8.
 433 The seasonal variation in air temperature in the oasis and desert was similar; however,
 434 the air temperature in the desert was generally higher than that in the oasis by

435 approximately 0.6 °C on average annually (approximately 0.4 °C in the plant growing
436 season). Instead, the relative humidity in the desert was lower than that in the artificial
437 oasis in the midstream region (approximately 9% and 10% in the annual and plant
438 growing seasons, respectively). The relative humidity in natural oasis and desert areas
439 are similar due to the extreme arid regions with rare precipitation, little irrigation
440 amount and small natural oasis area. Generally, the desert surface has the characteristics
441 of high temperature and lower humidity, and the oasis is a cold and wet island. In the
442 middle and lower reaches of the oasis and desert areas, the wind speed in the desert was
443 obviously larger than that in the oasis because of the wind shield effect in the oasis
444 (middle reaches: 1~3 m/s in the oasis, 2~6 m/s in the desert; lower reaches: 3~6 m/s in
445 the oasis, 3~7 m/s in the desert), and the wind speed decreased significantly when
446 passing by the windbreaks, buildings and crops, especially in the artificial oasis in the
447 middle reaches. The lower wind speed in oases is helpful to plant growth, people's
448 survival environment and the maintenance of oasis and desert ecosystems (Wang and
449 Cheng, 1999). While the seasonal variation in wind speed between desert and oasis was
450 similar, this indicated that they were controlled by the same synoptic system. The wind
451 speed in the natural oasis in the lower reaches was higher than that in the artificial oasis
452 in the middle reaches. The maximum wind speeds were observed in April in the
453 artificial and natural oases, respectively, while the minimum values were observed in
454 July. The air pressure decreased with decreasing elevation, e.g., the air pressure in the
455 middle reaches with relative high elevation was lower than that in the lower reaches, as
456 well as the discrete distribution of stations in the middle reaches with different

457 elevations (Fig. 10g and h, Table 1).

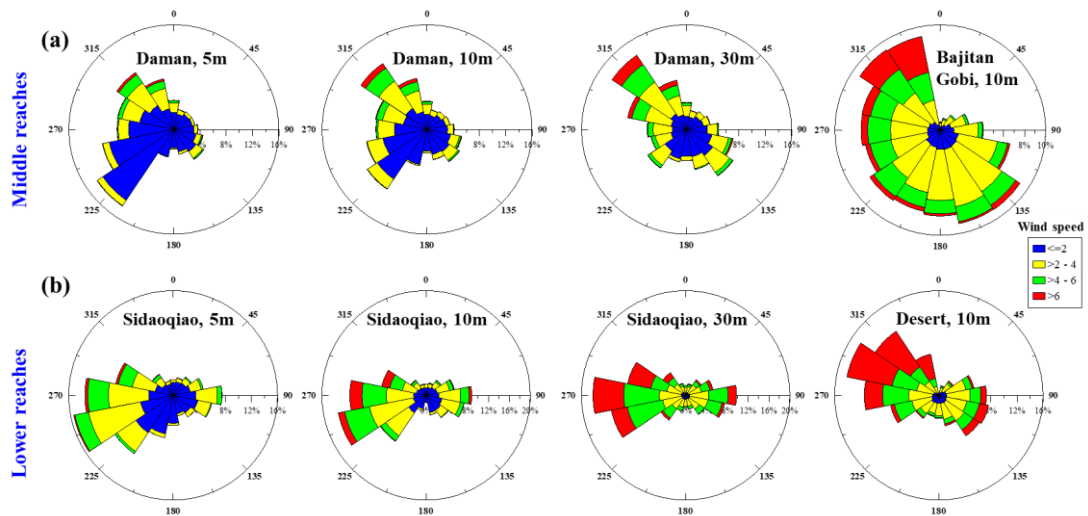


458

459 Fig. 8 Micrometeorological comparison between the oasis and desert (a, b: air
460 temperature; c, d: relative humidity; e, f: wind speed; g, h: air pressure, 2012-2021)

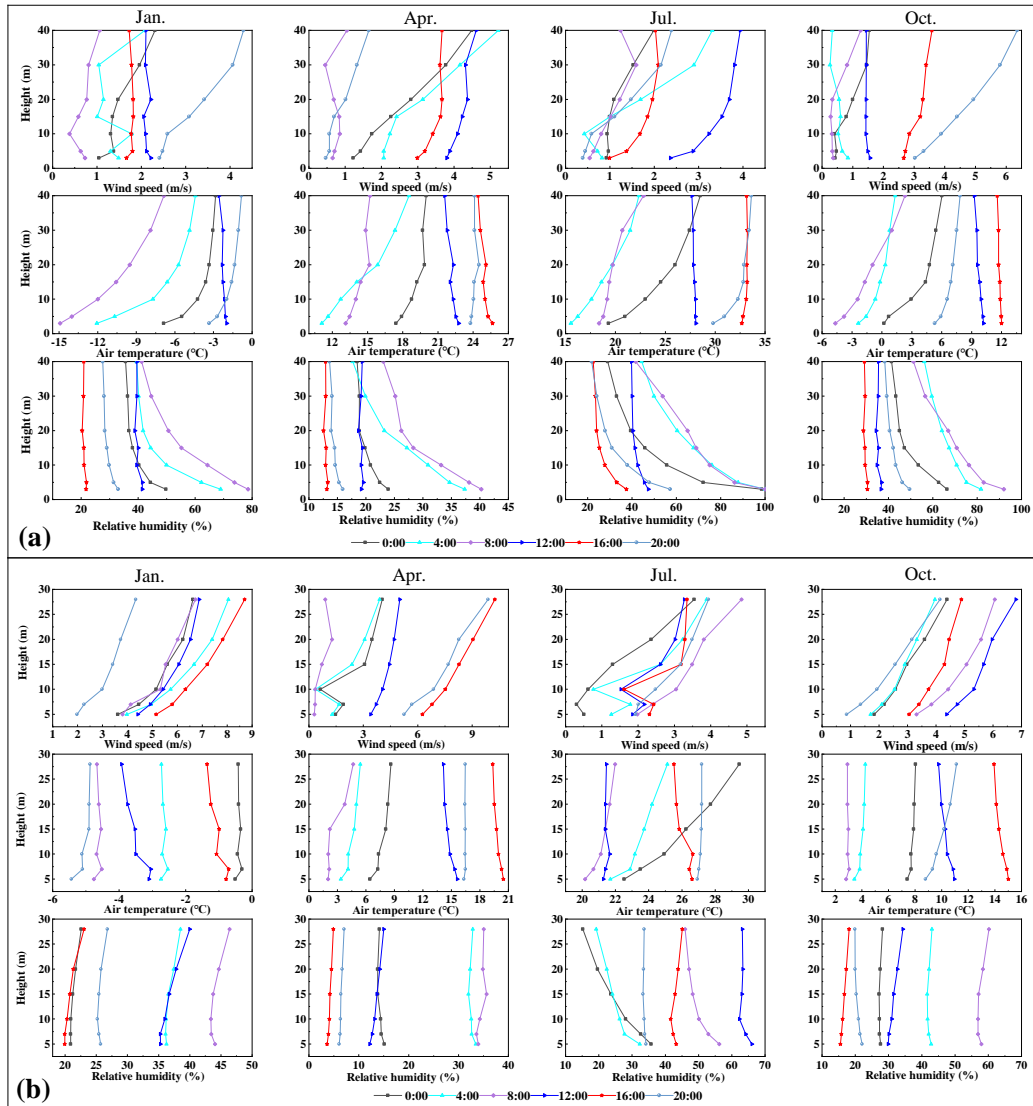
461 Windbreaks, buildings, crops or riparian forests drag on the wind flow inside the oasis,
462 and the wind direction is different in the oasis and desert. In the middle reaches, the
463 dominant wind directions in the desert are the northwest wind and southeast wind
464 directions, while they are northwest and southwest (10 m) in the oasis cropland;
465 however, with the increase in observation height, the influence of surface roughness on
466 wind speed/direction decreased, and the southwest wind gradually decreased, while the
467 northwest wind and southeast wind gradually increased, which is similar to the wind in
468 the desert area around the oasis (~30 m height). In the lower reaches, the wind direction

469 was similar in the oasis and desert areas, with prevailing wind directions of west and
 470 east (Fig. 9).



471
 472 Fig. 9 Wind speed/direction in the oasis and desert area (2012-2021) (a: artificial oasis-
 473 desert area in middle reaches; b: natural oasis-desert area in lower reaches; legend is
 474 wind speed)

475 There are six/seven layer gradient observations of wind, air temperature and
 476 humidity in superstations in artificial and natural oases. Data on typical days during
 477 January, April, July and October in 2021 were selected, and the profiles of wind speed,
 478 air temperature and humidity are plotted in Fig. 10. The wind speed generally increased
 479 with the observation height, especially in the natural oasis. The air temperature showed
 480 inversion at night during atmospheric stable stratification and changed little even below
 481 10 m in the afternoon in July at both artificial and natural oases, which may be caused
 482 by oasis-desert interactions. The relative humidity was low during the daytime and
 483 maintained high values at night, decreasing with the observation height, especially
 484 below 10 m.



485

486 Fig. 10 The profile of wind speed, air temperature and relative humidity in typical days
 487 of January 14, April 14, July 14 and October 14 in 2021 (a: artificial oasis in middle
 488 reaches; b: natural oasis in lower reaches)

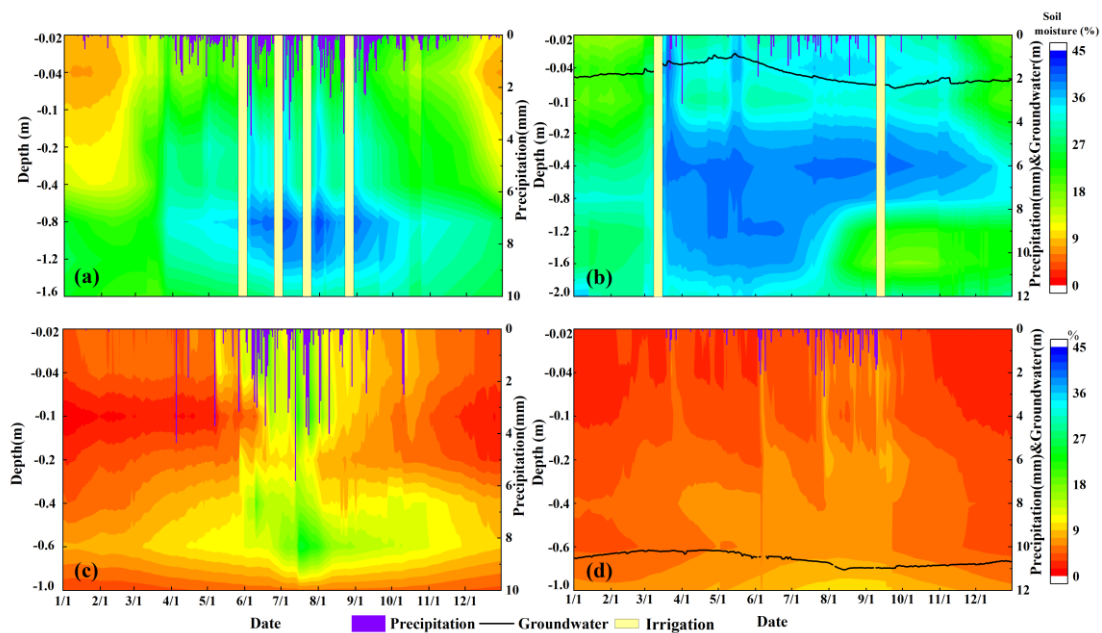
489 **4.2.3 Precipitation, soil moisture and groundwater table**

490 Figure 11 shows the variations in precipitation, soil moisture profiles and
 491 groundwater table (lower reaches) in typical oasis and desert ecosystems. Precipitation
 492 in the middle reaches was higher than that in the lower reaches, and it was higher in the
 493 oasis than in the desert. The soil moisture in the oasis was significantly higher than that

494 in the desert, and it was especially small in the desert of the lower reaches. The soil
495 moisture exhibited an increasing trend with increasing soil depth, especially in the oasis.
496 The soil moisture was higher at depths of 0.8-1 m in the artificial oasis in the middle
497 reaches and at depths of 0.4-0.8 m in the natural oasis in the lower reaches. Soil crust
498 appeared in the lower reaches due to soil salinization, and it may prevent the loss of soil
499 moisture. When a precipitation event occurred, the soil moisture in the desert increased
500 accordingly; however, there were no clear variations in the oasis. There were usually
501 four irrigation events in the artificial oasis in the middle reaches, and the soil moisture
502 increased clearly accordingly, while some occasional peaks in soil moisture were due
503 to relative heavy precipitation (Fig. 11a). In the lower reaches, two irrigation events
504 (usually in March and September) generally occurred in riparian forests in natural oases.
505 The shallow soil moisture showed large values in March when irrigation occurred and
506 decreased in the plant growing season with a slight increase in September. Another
507 phenomenon is that the precipitation in the artificial oasis was larger than that in the
508 desert, although the sites were not far away from each other (e.g., 103.1 mm at the
509 Daman superstation and 75.4 mm at the Gobi station). From the analysis, the soil
510 moisture in the desert was strongly dependent on precipitation (Fig. 11c, d), while it
511 maintained high values in the plant growth season relying on irrigation in the oasis.

512 In the lower reaches, five systems for groundwater table measurement have operated
513 since June 2014 in the oasis, near the Sidaoqiao, Mixed Forest, *Populus euphratica*,
514 Cropland, and Barren Land stations. The groundwater table was approximately 1–3 m
515 under the ground, and the groundwater table level declined from a depth of

516 approximately 1 m to 3 m in the growing season to supply the riparian forest growth
 517 (Fig. 11b). Additionally, one groundwater table measurement system was installed near
 518 the desert station in 2018. The depth of the groundwater table level was approximately
 519 10-11 m in the desert and showed no significant variation over the years (Fig. 11d).

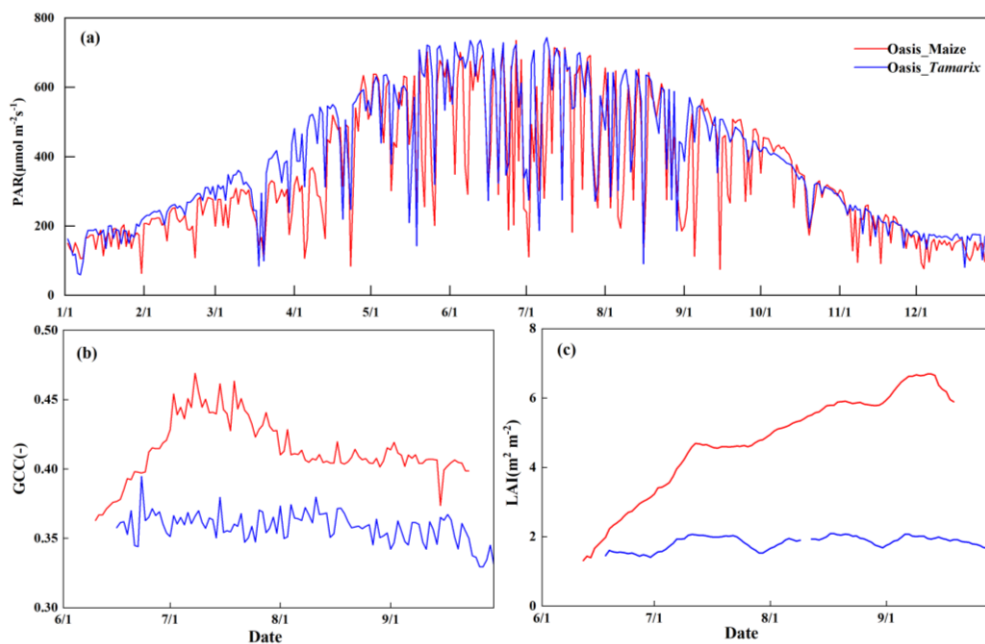


520
 521 Fig. 11. Comparison of precipitation and soil moisture profile between desert and oasis
 522 (2012-2021, a: oasis in the middle reaches (maize, Daman); b: oasis in the lower reaches
 523 (*Tamarix*, Sidaoqiao); c: desert in middle reaches (Bajitan Gobi); d: desert in lower
 524 reaches (desert))

525 4.3 Vegetation and soil parameters

526 The vegetation parameters include photosynthetically active radiation (PAR), leaf
 527 area index (LAI), phenology, sun-induced chlorophyll fluorescence (SIF), etc. The PAR,
 528 the amount of light available for photosynthesis, is observed at stations with vegetation
 529 cover, and it can be used as the source of energy for photosynthesis by green plants.

530 The PAR observations showed similar seasonal variations in typical oasis ecosystems
 531 in the middle and lower reaches, with a maximum daily PAR of approximately 750
 532 $\mu\text{mol m}^{-2} \text{s}^{-1}$ (Fig. 14a). Vegetation parameters, such as LAI and phenology, were also
 533 observed in the middle and lower reaches. LAI in the middle reaches (maize) increased
 534 gradually with crop growth, and it was larger than that in the lower reaches (*Tamarix*),
 535 which showed little change in this shrub surface (Fig. 14b). The phenological camera
 536 was installed at each station except the desert to acquire the phenology. The greenness
 537 index of the green chromatic coordinate (GCC) was derived to capture the key
 538 phenological phase of the plant, such as the SOS (start of season), POP (position of
 539 peak value), and EOS (end of season) (Fig. 14c).



540
 541 Fig. 12. Variations in vegetation parameters in the middle and lower reaches of the oasis
 542 (a, b, c are PAR, LAI and GCC in the artificial and natural oases, respectively, in 2018)

543 Soil samples were collected at each station in the middle and lower reaches in 2012
 544 and 2020. These soil samples were analyzed in the laboratory, and parameters such as

545 soil texture, porosity, bulk density, saturated hydraulic conductivity, and soil organic
 546 matter content were obtained. Some soil parameters at typical stations are shown in
 547 Table 3. Silty soil is dominant in the oasis, and sand is dominant in the desert. The
 548 porosity and bulk density showed no significant difference. The saturated hydraulic
 549 conductivity and soil organic matter at the typical stations are also given in Table 3.

550 Table 3 Soil parameter measurements at typical stations in 2020

	Station	Soil texture	Soil properties
Middle reaches	Daman (Oasis)	Clay: 6% Silt: 69% Sand: 25%	Porosity: 47.1 %; Bulk density: 1.46 g/cm ³ ; Saturated hydraulic conductivity: 0.177 mm/min; Saturated water capacity: 64.10 %; PH: 8.48; NH ₄ ⁺ -N: 0.83 mg/kg; NO ₃ ⁻ -N: 15.90 mg/kg; Soil carbon content: 1.85 %; Soil organic carbon content: 0.72 %; Soil nitrogen content: 0.027%
	Huaizhaizi (Desert)	Clay: 1% Silt: 19% Sand: 80%	Porosity: 38.0 %; Bulk density: 1.49 g/cm ³ ; Saturated hydraulic conductivity: 4.93 mm/min; Saturated water capacity: 22.21 %; PH: 8.27; NH ₄ ⁺ -N: 0.77 mg/kg; NO ₃ ⁻ -N: 29.70 mg/kg; Soil carbon content: 1.83 %; Soil organic carbon content: 0.33 %; Soil nitrogen content: 0.026%
Lower reaches	Sidaoqiao (Oasis)	Clay: 21% Silt: 69% Sand: 10%	Porosity: 45.8 %; Bulk density: 1.47 g/cm ³ ; PH: 8.80; NH ₄ ⁺ -N: 1.02 mg/kg; NO ₃ ⁻ -N: 5.23 mg/kg; Soil carbon content: 2.02 %; Soil organic carbon content: 0.70 %; Soil nitrogen content: 0.070%
	Desert around terminal lake (Desert)	Clay: 9% Silt: 7% Sand: 84%	Porosity: 44.4 %; Bulk density: 1.49 g/cm ³ ; PH: 8.62; NH ₄ ⁺ -N: 0.26 mg/kg; NO ₃ ⁻ -N: 5.74 mg/kg; Soil carbon content: 1.42 %; Soil organic carbon content: 0.38 %; Soil nitrogen content: 0.039%

551 **5. Data availability**

552 The dataset of energy, water vapor and carbon exchange observations in oasis-desert
 553 areas reported in this study, including energy, water vapor and carbon fluxes,
 554 hydrometeorological data, and vegetation and soil parameters, are available and can be
 555 downloaded freely at the National Tibetan Plateau Data Center
 556 (<https://doi.org/10.11888/Terre.tpdc.300441>, Liu et al., 2023). A specific directory for
 557 each observation station was designated with data classified into three categories,
 558 namely, energy, water vapor and carbon fluxes, hydrometeorological data, and

559 vegetation and soil parameter data. Short descriptions were also provided for each
560 dataset. The Beijing standard time was used in all the data files (UTC+8).

561 **6. Conclusions**

562 The typical land covers in the middle and lower reaches over the HRB are oases and
563 deserts characterized by fragile environments. Oasisization and desertification are two
564 opposing processes in arid and semiarid regions with scarce water resources. To combat
565 desertification around oases and maintain the sustainable development of oases, a land
566 surface process integrated observatory network was established in the oasis-desert area
567 in the middle and lower reaches of the HRB. Eleven stations (7 in oasis, 4 in desert)
568 have been established in these regions since 2012 to monitor the energy, water vapor
569 and carbon exchange between land and atmosphere over oasis and desert areas, and a
570 long-term and high-quality oasis and desert dataset of energy, water vapor and carbon
571 fluxes and auxiliary parameters was produced. This study shows the achievements of
572 11 stations over 10 continuous years of observations, including energy, water vapor and
573 carbon fluxes, hydrometeorology, vegetation and soil parameter data. These data can
574 be used in the analysis of the water-heat-carbon process and its influence mechanism
575 (Wang et al., 2019; Xu et al., 2020; Bai et al., 2021; Wu et al., 2023), calibration and
576 validation of remote sensing products (Ma et al., 2018; Song et al., 2018; Li et al., 2021;
577 Zhang et al., 2022), and simulations of energy, water vapor and carbon exchange (Li et
578 al., 2017b; Liu et al., 2020; He et al., 2022; Zhou et al., 2022). We confirm that the 10-
579 year long-term dataset presented in this study is of high quality with few missing data
580 and believe that the datasets will support ecological security and sustainable

581 development in oasis-desert areas. Most of the stations are ongoing observations, which
582 can play a greater role in such ecologically fragile areas and provide a reference for
583 other similar oasis-desert areas along the Silk Road.

584

585 **Acknowledgement**

586 This work was supported by the Strategic Priority Research Program of the Chinese
587 Academy of Sciences (Grant no. XDA20100101), the National Natural Science
588 Foundation of China (42171461).

589

590 **References:**

591 Bai, Y., Liu, Y. L., Kueppers, L. M., Feng, X., Yu, K. L., Yang, X. F., Li, X. Y., and
592 Huang, J. P.: The coupled effect of soil and atmospheric constraints on stress-
593 responses of desert riparian species, *Agr. Forest Meteorol.*, 311, 108701,
594 <https://doi.org/10.1016/j.agrformet.2021.108701>, 2021.

595 Che, T., Dai, L.Y., Wang, J., Zhao, K., and Liu, Q: Estimation of snow depth and snow
596 water equivalent distribution using airborne microwave radiometry in the Binggou
597 Watershed, the upper reaches of the Heihe River basin, *Int. J. Appl. Earth Obs.*, 17,
598 23-32, <https://doi.org/10.1016/j.jag.2011.10.014>, 2012.

599 Che, T., Li, X., Liu, S.M., Li, H.Y., Xu, Z.W., Tan, J.L., Zhang, Y., Ren, Z.G., Xiao, L.,
600 Deng, J., Jin, R., Ma, M.G., Wang, J., and Yang, X.F.: Integrated hydrometeorological,
601 snow and frozen-ground observations in the alpine region of the Heihe River Basin,
602 China, *Earth Syst. Sci. Data*, 11, 1483–1499, 2019.

603 Cheng, G. D., Xiao, D. N., and Wang, G. X.: On the characteristics and building of

604 landscape ecology in arid area, *Adv. Geosci.*, 14 (1), 11–15, 1999. (in Chinese with
605 English abstract).

606 Cheng, G. D., Li, X., Zhao, W., Xu, Z., Feng, Q., Xiao, S. and Xiao, H.: Integrated study
607 of the water-ecosystem-economy in the Heihe River Basin, *Natl. Sci. Rev.*, 1(3), 413-
608 428, <https://doi.org/10.1093/nsr/nwu017>, 2014.

609 Chu, P. C., Lu, S., and Chen, Y.: A numerical modeling study on desert oasis self-
610 supporting mechanisms, *J. Hydrol.*, 312, 256-276,
611 <https://doi.org/10.1016/j.jhydrol.2005.02.043>, 2005.

612 Crétaux, J. F., Calmant, S., Romanovski, V., Shabunin, A., Lyard, F., Bergé-Nguyen,
613 M., Cazenave, A., Hernandez, F., and Perosanz, F.: An absolute calibration site for
614 radar altimeters in the continental domain: Lake Issykkul in the central Asia, *J.*
615 *Geodesy*, 83(8), 723-735, <http://doi.org/10.1007/s00190-008-0289-7>, 2009.

616 Dregne, H. E.: Global status of desertification, *Annals of Arid Zone*, 30, 179–185,
617 <https://epubs.icar.org.in/index.php/AAZ/article/view/64733>, 1991.

618 Georgescu, M., Moustouli, M., Mahalov, A., and Dudhia, J.: An alternative explanation
619 of the semiarid urban area “oasis effect”, *J. Geophys. Res.-Atmos.*, 116, D24113,
620 <https://doi.org/10.1029/2011JD016720>, 2011.

621 He, X. L., Liu, S. M., Xu, T. R., Yu, K. L., Gentile, P., Zhang, Z., Xu, Z. W., Jiao, D.
622 D., and Wu, D. X.: Improving predictions of evapotranspiration by integrating multi-
623 source observations and land surface model, *Agr. Water Manage.*, 272, 107827,
624 <https://doi.org/10.1016/j.agwat.2022.107827>, 2022.

625 Hommeltenberg, J., Mauder, M., Drosler, M., Heidbach, K., Werle, P., and Schmid, H.

626 P.: Ecosystem scale methane fluxes in a natural temperature bog-pine forest in
627 southern Germany, *Agric. For. Meteorol.*, 198–199, 273–284,
628 <https://doi.org/10.1016/j.agrformet.2014.08.017>, 2014.

629 Huang, J. P., Yu, H. P., Guan, X. D., Wang, G. Y., and Guo, R. X: Accelerated dryland
630 expansion under climate change, *Nature Clim. Change*, 6, 166–171,
631 <https://doi.org/10.1038/nclimate2837>, 2016.

632 Liebethal, C., Huwe, B., and Foken, T.: Sensitivity analysis for two ground heat flux
633 calculation approaches, *Agric. For. Meteorol.*, 132(3–4), 253–262,
634 <https://doi.org/10.1016/j.agrformet.2005.08.00>, 2005.

635 Li, M. S., Zhou, J., Peng, Z. X., Liu, S. M., Göttsche, F. M., Zhang, X. D., and Song, L.
636 S.: Component radiative temperatures over sparsely vegetated surfaces and their
637 potential for upscaling land surface temperature, *Agric. For. Meteorol.*, 276–277,
638 107600, <https://doi.org/10.1016/j.agrformet.2019.05.031>, 2019.

639 Li, X., Li, X. W., Li, Z. Y., Ma, M. G., Wang, J., Xiao, Q., Liu, Q., Che, T., Chen, E. X.,
640 Yan, G. J., Hu, Z. Y., Zhang, L. X., Chu, R. Z., Su, P. X., Liu, Q. H., Liu, S. M.,
641 Wang, J. D., Niu, Z., Chen, Y., Jin, R., Wang, W. Z., Ran, Y. H., and Xin, X.:
642 Watershed Allied Telemetry Experimental Research, *J. Geophys. Res.-Atmos.*,
643 114, D22103, <https://doi.org/10.1029/2008JD011590>, 2009.

644 Li, X., Cheng, G. D., Liu, S. M., Xiao, Q., Ma, M. G., Jin, R., Che, T., Liu, Q. H., Wang,
645 W. Z., Qi, Y., Wen, J. G., Li, H. Y., Zhu, G. F., Guo, J. W., Ran, Y. H., Wang, S. G.,
646 Zhu, Z. L., Zhou, J., Hu, X. L., and Xu, Z. W.: Heihe Watershed Allied Telemetry
647 Experimental Research (HiWATER): Scientific Objectives and Experimental

648 Design, B. Am. Meteorol. Soc., 94, 1145–1160, <https://doi.org/10.1175/BAMS-D->
649 12-00154.1, 2013.

650 Li, X., Yang, K., and Zhou, Y.: Progress in the study of oasis-desert interactions, Agric.
651 For. Meteorol., 230, 1-7, <https://doi.org/10.1016/j.agrformet.2016.08.022>, 2016.

652 Li, X., Liu, S. M., Xiao, Q., Ma, M. G., Jin, R., Che, T., Wang, W. Z., Hu, X. L., Xu, Z.
653 W., Wen, J. G., and Wang, L. X.: A multiscale dataset for understanding complex
654 eco-hydrological processes in a heterogeneous oasis system, Sci. Data, 4, 170083,
655 <https://doi.org/10.1038/sdata.2017.83>, 2017a.

656 Li, X., Zheng, Y., Sun, Z., Tian, Y., Zheng, C. M., Liu, J., Liu, S. M., and Xu, Z. W.: An
657 integrated ecohydrological modeling approach to exploring the dynamic
658 interaction between groundwater and phreatophytes, Ecol. Model., 356, 127-140,
659 <https://doi.org/10.1016/j.ecolmodel.2017.04.017>, 2017b.

660 Li, X., Liu, S. M., Li, H. X., Ma, Y. F., Wang, J. H., Zhang, Y., Xu, Z. W., Xu, T. R.,
661 Song, L. S., Yang, X. F., Lu, Z., Wang, Z. Y., and Guo, Z. X.: Intercomparison of
662 six upscaling evapotranspiration methods: from site to the satellite pixel, J.
663 Geophys. Res.-Atmos., 123, 6777-6803, <https://doi.org/10.1029/2018JD028422>,
664 2018.

665 Li, X., Liu, S. M., Yang, X. F., Ma, Y. F., He, X. L., Xu, Z. W., Xu, T. R., Song, L. S.,
666 Zhang, Y., Hu, X., Qu, Q., and Zhang, X. D.: Upscaling evapotranspiration from a
667 single-site to satellite pixel scale, Remote Sen., 13, 4072,
668 <https://doi.org/10.3390/rs13204072>, 2021.

669 Liu, R., Sogachev, A., Yang, X. F., Liu, S. M., Xu, T. R., and Zhang, J. J.: Investigating

670 microclimate effects in an oasis-desert interaction zone, *Agric. For. Meteorol.*, 290,
671 107992, <https://doi.org/10.1016/j.agrformet.2020.107992>, 2020.

672 Liu, S. M., Xu, Z. W., Wang, W. Z., Bai, J., Jia, Z. Z., Zhu, M. J., and Wang, J. M.: A
673 comparison of eddy-covariance and large aperture scintillometer measurements
674 with respect to the energy balance closure problem. *Hydrol. Earth Syst. Sci.*, 15(4),
675 1291-1306, <https://doi.org/10.5194/hess-15-1291-2011>, 2011.

676 Liu, S. M., Xu, Z. W., Song, L. S., Zhao, Q. Y., Ge, Y., Xu, T. R., Ma, Y. F., Zhu, Z. L.,
677 Jia, Z. Z., and Zhang, F.: Upscaling evapotranspiration measurements from multi-
678 site to the satellite pixel scale over heterogeneous land surfaces, *Agric. For.*
679 *Meteorol.*, 230-231, 97-113, <https://doi.org/10.1016/j.agrformet.2016.04.008>,
680 2016.

681 Liu, S. M., Li, X., Xu, Z. W., Che, T., Xiao, Q., Ma, M. G., Liu, Q. H., Jin, R., Guo, J.
682 W., Wang, L. X., Wang, W. Z., Qi, Y., Li, H. Y., Xu, T. R., Ran, Y. H., Hu, X. L.,
683 Shi, S. J., Zhu, Z. L., Tan, J. L., Zhang, Y., and Ren, Z.G.: The Heihe Integrated
684 Observatory Network: A basin-scale land surface processes observatory in China,
685 *Vadose Zone J.*, 17, 180072, <https://doi.org/10.2136/vzj2018.04.0072>, 2018.

686 Liu, S., Xu, Z., Che, T., Li, X., Xu, T., Ren, Z., Zhang, Y., Tan, J., Song, L., Zhou, J.,
687 Zhu, Z., Yang, X., Liu, R., and Ma, Y.: Energy, water vapor and carbon exchange
688 observations in oasis-desert areas of Heihe river basin (2012-2021), National
689 Tibetan Plateau/Third Pole Environment Data Center,
690 <https://doi.org/10.11888/Terre.tpdc.300441>, 2023.

691 Ma, Y. F., Liu, S. M., Song, L. S., Xu, Z. W., Liu, Y. L., Xu, T. R., and Zhu, Z. L.:

692 Estimation of daily evapotranspiration and irrigation water efficiency at a Landsat-
693 like scale for an arid irrigation area using multi-source remote sensing data, *Remote*
694 *sens. environ.*, 216, 715-734, <https://doi.org/10.1016/j.rse.2018.07.019>, 2018.

695 Mao, D., Wang, Z., Wu, B., Zeng, Y., Luo, L., and Zhang, B: Land degradation and
696 restoration in the arid and semiarid zones of China: Quantified evidence and
697 implications from satellites. *Land degrad, Dev.*, 29(11), 3841-3851,
698 <https://doi.org/10.1002/ldr.3135>, 2018.

699 Meng, X., Lv, S., Zhang, T., Guo, J., Gao, Y., Bao, Y., Wen, L., Luo, S., and Liu, Y.:
700 Numerical simulations of the atmospheric and land conditions over the jinta oasis in
701 northwestern China with satellite-derived land surface parameters, *J. Geophys. Res.-*
702 *Atmos.*, 114, 605-617, <https://doi.org/10.1029/2008JD010360>, 2009.

703 Potchter, O., Goldman, D., Kadish, D., and Iluz, D.: The oasis effect in an extremely
704 hot and arid climate: The case of southern Israel, *J. Arid Environ.*, 72, 1721-1733,
705 <https://doi.org/10.1016/j.jaridenv.2008.03.004>, 2008.

706 Qu, Y. H., Zhu, Y. Q., Han, W. C., Wang, J. D., and Ma, M. G: Crop leaf area index
707 observations with a wireless sensor network and its potential for validating remote
708 sensing products, *IEEE J-STARS.*, 7(2), 431-444,
709 <https://doi.org/10.1109/JSTARS.2013.2289931>, 2014.

710 Scanlon, B. R., Keese, K. E., Flint, A. L., Flint, L. E., Gaye, C. B., Edmunds, W. M.,
711 and Simmers, I.: Global synthesis of groundwater recharge in semiarid and arid
712 regions, *Hydrol. Process*, 20 (15), 3335–3370, <https://doi.org/10.1002/hyp.6335>,
713 2006.

714 Stone, K. B.: Burke-Litwin organizational assessment survey: reliability and validity,
715 Organization development journal, 33(2), 33-50, 2015.

716 Stanev, E., Staneva, J., Bullister, J., and Murray, J.: Ventilation of the black sea
717 pycnocline. Parameterization of convection, numerical simulations and validations
718 against observed chlorofluorocarbon data, Deep sea research part I: Oceanographic
719 research papers, 51 (12), 2137-2169, <https://doi.org/10.1016/j.dsr.2004.07.018>, 2004.

720 Stoy, P.C., Mauder, M., Foken, T., Marcolla, B., Boegh, E., Ibrom, A., Arain, M., Arneth,
721 A., Aurela, M., Bernhofer, C., Cescatti, A., Dellwik, E., Duce, P., Gianelle, D., Gorsel,
722 E., Kiely, G., Knohl, A., Margolis, H., McCaughey, H., Merbold, L., Montagnanti,
723 L., Papale, D., Reichstein, M., Saunders, M., Serrano-Ortiz, P., Sottocornola, M.,
724 Spano, D., Vaccari, F., and Varlagin, A: A data-driven analysis of energy balance
725 closure across FLUXNET research sites: The role of landscape scale heterogeneity,
726 Agric. For. Meteorol., 171-172, 137-152,
727 <http://dx.doi.org/10.1016/j.agrformet.2012.11.004>, 2013.

728 Song, L.S., Liu, S.M., Kustas, W.P., Nieto, H., Sun, L., Xu, Z.W., Skaggs, T.H., Yang,
729 Y., Ma, M.G., Xu, T.R., Tang, X.G., and Li, Q.P.: Monitoring and validating spatially
730 and temporally continuous daily evaporation and transpiration at river basin scale,
731 Remote sens. environ., 219, 72-88, <https://doi.org/10.1016/j.rse.2018.10.002>, 2018.

732 Taha, H., Akbari, H., and Rosenfeld, A.: Heat island and oasis effects of vegetative
733 canopies, Theor. Appl. Climatol., 44, 123-138, <https://doi.org/10.1007/BF00867999>,
734 1991.

735 Tagesson, T., Fensholt, R., Cappelaere, B., Mougín, E., Horion, S., Kergoat, L., Nieto,

736 H., Mbow, C., Ehammer, A., Demarty, J., and Ardö, J.: Spatiotemporal variability in
737 carbon exchange fluxes across the Sahel, *Agric. For. Meteorol.*, 226-227, 108-118,
738 <https://doi.org/10.1016/j.agrformet.2016.05.013>, 2016.

739 Twine, T.E., Kustas, W.P., Norman, J.M., Cook, D.R., Houser, P.R., Meyers, T.P.,
740 Prueger, J.H., Starks, P.J., and Wesely, M.L.: Correcting eddy-covariance flux
741 underestimates over a grassland. *Agric. For. Meteorol.*, 103(3), 279-300,
742 [https://doi.org/10.1016/S0168-1923\(00\)00123-4](https://doi.org/10.1016/S0168-1923(00)00123-4), 2000.

743 Wang, J. M., and Mitsuta, Y.: Evaporation from the desert: some preliminary results of
744 HEIFE, *Boundary Layer Meteorology*, 59, 413-418,
745 <https://doi.org/10.1007/BF0221546>, 1992.

746 Wang, G. X., and Cheng, G. D.: Water resource development and its influence on the
747 environment in arid areas of China-the case of the Hei River basin, *J. Arid Environ.*,
748 43, 121–131, <https://doi.org/10.1006/jare.1999.0563>, 1999.

749 Wang, H. B., Li, X., Xiao, J. F., Ma, M. G., Tan, J. L., Wang, X. F., and Geng, L. Y.:
750 Carbon fluxes across alpine, oasis, and desert ecosystems in northwestern China: The
751 importance of water availability, *Sci. total environ.*, 697, 133978,
752 <https://doi.org/10.1016/j.scitotenv.2019.133978>, 2019.

753 Wen, X., Lv, S., and Jin, J.: Integrating remote sensing data with WRF for improved
754 simulations of oasis effects on local weather processes over an arid region in
755 northwestern China, *J. Hydrometeorol.*, 13(2), 573-587,
756 <https://doi.org/10.1175/JHM-D-10-05001.1>, 2012.

757 Wu, D. X., Liu, S. M., Wu, X. C., Xu, T. R., Xu, Z. W., He, X. L., and Shi, H. Y.:

758 Evaluation of the intrinsic temperature sensitivity of ecosystem respiration in typical
759 ecosystems of an endorheic river basin, *Agric. For. Meteorol.*, 333, 109393,
760 <https://doi.org/10.1016/j.agrformet.2023.109393>, 2023.

761 Xu, Z. W., Liu, S. M., Li, X., Shi, S. J., Wang, J. M., Zhu, Z. L., Xu, T. R., Wang, W.
762 Z., and Ma, M. G.: Intercomparison of surface energy flux measurement systems
763 used during the HiWATER-MUSOEXE, *J. Geophys. Res.-Atmos.*, 118, 13140-
764 13157, <https://doi.org/10.1002/2013JD020260>, 2013.

765 Xu, Z.W., Ma, Y.F., Liu, S.M., Shi, W.J., and Wang, J.M.: Assessment of the energy
766 balance closure under advective conditions and its impact using remote sensing data,
767 *J. Appl. Meteorol. Clim.*, 56 (1), 127-140, [https://doi.org/10.1175/JAMC-D-16-](https://doi.org/10.1175/JAMC-D-16-0096.1)
768 0096.1, 2017.

769 Xu, Z. W., Liu, S. M., Zhu, Z. L., Zhou, J., Shi, W. J., Xu, T. R., Yang, X. F., Zhang, Y.,
770 and He, X.L.: Exploring evapotranspiration changes in a typical endorheic basin
771 through the integrated observatory network, *Agric. For. Meteorol.*, 290, 108010,
772 <https://doi.org/10.1016/j.agrformet.2020.108010>, 2020.

773 Xue, J., Gui, D., Lei, J., Sun, H., Zeng, F., Mao, D., Zhang, Z., Jin, Q., and Liu, Y.:
774 Oasis microclimate effects under different weather events in arid or hyper arid
775 regions: A case analysis in southern Taklimakan desert and implication for
776 maintaining oasis sustainability, *Theor. Appl. Climatol.*, 137, 89-101,
777 <https://doi.org/10.1007/s00704-018-2567-5>, 2019.

778 Zhang, Y. Y., and Zhao, W. Z.: Vegetation and soil property response of short-
779 timefencing in temperate desert of the Hexi Corridor northwestern China, *Catena*,

780 133, 43–51, <https://doi.org/10.1016/j.catena.2015.04.019>, 2015.

781 Zhang, X. Y., Arimoto, R., Zhu, G. H., Chen, T., and Zhang, G. Y.: Concentration, size-
782 distribution and deposition of mineral aerosol over Chinese desert regions, *Tellus B:*
783 *Chemical and Physical Meteorology*, 50(4), 317-330,
784 <https://doi.org/10.3402/tellusb.v50i4.16131>, 2016a.

785 Zhang, Q., Sun, R., Jiang, G.Q., Xu, Z. W., and Liu, S. M.: Carbon and energy flux
786 from a *Phragmites australis* wetland in Zhangye oasis-desert area, China, *Agric. For.*
787 *Meteorol.*, 230-231, 45-57, <https://doi.org/10.1016/j.agrformet.2016.02.019>, 2016b.

788 Zhang, Y., Zhao, W., He, J., and Fu, L.: Soil susceptibility to macropore flow across a
789 desert-oasis ecotone of the Hexi Corridor, Northwest China, *Water Resour. Res.*, 54,
790 1281–1294, <https://doi.org/10.1002/2017WR021462>, 2018.

791 Zhang, Z., Poulter, B., Knox, S., Stavert, A., McNicol, G., Fluet-Chouinard, E.,
792 Feinberg, A., Zhao, Y., Bousquet, P., Canadell, J., Ganesan, A., Hugelius, G., Jackson,
793 R., Patra, P., Saunio, M., Höglund-Isaksson, L., Huang, C., Chatterjee, A., and Li,
794 X.: Anthropogenic emission is the main contributor to the rise of atmospheric
795 methane during 1993–2017, *Natl. Sci. Rev.*, 9(5), nwab200,
796 <https://doi.org/10.1093/nsr/nwab200>, 2022.

797 Zhang, Y., Liu, S. M., Song, L. S., Li, X., Jia, Z. Z., Xu, T. R., Xu, Z. W., Ma, Y. F.,
798 Zhou, J., Yang, X. F., He, X. L., Yao, Y. J., and Hu, G. C.: Integrated Validation of
799 Coarse Remotely Sensed Evapotranspiration Products over Heterogeneous Land
800 Surfaces, *Remote Sens.*, 14, 3467, <https://doi.org/10.3390/rs14143467>, 2022.

801 Zhao, R., Chen, Y., Shi, P., Zhang, L., Pan, J., and Zhao, H.: Land use and land cover

802 change and driving mechanism in the arid inland river basin: a case study of Tarim
803 River, Xinjiang, China, *Environ. Earth sci.*, 68(2), 591-604, [https://doi](https://doi.org/10.1007/s12665-012-1763-3)
804 [10.1007/s12665-012-1763-3](https://doi.org/10.1007/s12665-012-1763-3), 2013.

805 Zheng, C., Liu, S. M., Song, L. S., Xu, Z. W., Guo, J. X., Ma, Y. F., Ju, Q., and Wang,
806 J. M.: Comparison of sensible and latent heat fluxes from optical-microwave
807 scintillometers and eddy covariance systems with respect to surface energy balance
808 closure, *Agric. For. Meteorol.*, 331, 109345,
809 <https://doi.org/10.1016/j.agrformet.2023.109345>, 2023.

810 Zhou, Y., and Li, X.: Energy balance closures in diverse ecosystems of an endorheic
811 river basin, *Agric. For. Meteorol.*, 274, 118-131,
812 <https://doi.org/10.1016/j.agrformet.2019.04.019>, 2018.

813 Zhou, Y., Liao, W., and Li, X.: The contributions of individual factors to the oasis cold
814 island effect intensity in the Heihe River Basin, *Agric. For. Meteorol.*, 312, 108706,
815 <https://doi.org/10.1016/j.agrformet.2021.108706>, 2022.